Geochimica et Cosmochimica Acta 349 (2023) 41–54

Contents lists available at ScienceDirect

Geochimica et Cosmochimica Acta

journal homepage: www.elsevier.com/locate/gca

Carbonatite formation in continental settings via high pressure – high temperature liquid immiscibility

Márta Berkesi [a,b], Justine L. Myovela [c,d], Gregory M. Yaxley [e], Tibor Guzmics [a,*]

[a] Lithosphere Fluid Research Lab, Institute of Geography and Earth Sciences, Eötvös University Budapest, 1117 Pázmány Péter sétány 1/c, Hungary
[b] MTA-EPSS FluidsByDepth Lendület Research Group, Institute of Earth Physics and Space Science (EPSS), Eötvös Loránd Research Network, Sopron, 9400 Csatkai Endre utca 6-8, Hungary
[c] Institute of Geography and Earth Sciences, Department of Geology and Meteorology, Faculty of Sciences, University of Pécs, Ifjúság u. 6, Pécs 7624, Hungary
[d] College of Earth Sciences and Engineering, Department of Geology, University of Dodoma, P. O. Box, 11090, Dodoma, Tanzania
[e] Research School of Earth Sciences, Australian National University, Building 142, Mills Road, Acton, ACT 2601, Australia

ARTICLE INFO

Article history:
Received 14 October 2022
Accepted 22 March 2023
Available online 28 March 2023
Associate editor: Bernard Charlier

Keywords:
Carbonatite
Melilitite
Immiscibility
Melt inclusions

ABSTRACT

The goal of this study is to compare compositions of high temperature silicate-carbonatite immiscible melts, known from melt inclusions and experiments, to compositions of silica-undersaturated volcanic rocks from continental settings, in order to improve understanding of the formation of calcite carbonatite rocks worldwide. Melt inclusions in this study are abundant in perovskites crystals from magnetite-perovskite cumulates sampled at the Kerimasi volcano in the East African Rift System. The temperature of complete dissolution of daughter minerals in the melt inclusions and the high CO_2–content of the silicate melt (5.4–9.8 wt%) support early formation of the rock and entrapment of melts at high temperatures (~1100 °C) and pressures (≥1 GPa). Heated-quenched melt inclusions indicate the presence of immiscible mafic-melilitite and Ca-Na-K-carbonatite melts together with a fluid phase at entrapment. Melilitite melts are low in SiO_2 (29.4–33.5 wt%), moderate in MgO (4.0–5.9 wt%) but high in CaO (16.3–24.4 wt%), FeO^T (9.0–13.5 wt%), Na_2O (6.8–12.7 wt%) and K_2O (1.8–3.2 wt%). Coexisting carbonatite melts also show high CaO-content (28.4–39.0 wt%), along with moderate-to-high Na_2O (8.2–20.2 wt%) + K_2O (4.1–6.6 wt%) compositions (total alkalis ranges between 13.1 and 24.3 wt%).

We compared the studied silicate melts in the inclusions with a global dataset of 146 continental melilitite and 640 nephelinite compositions (GEOROC database). We argue that the studied calcite-saturated melilitite melts formed in a continental rift setting and were able to exsolve carbonatite melts that crystallized voluminous calcite carbonatite rocks during their evolution. In contrast, magnesian melilitite and nephelinite volcanic rocks from intracontinental settings are compositionally far away from any immiscibility field at feasible pressures and were only able to unmix carbonatite melts during late-stage evolution, leaving little opportunity for calcite crystallization. CaO- and alkali-rich, but extremely SiO_2-undersaturated melilitite melts play a key role in early silicate-carbonatite immiscibility, can only be preserved in melt inclusions and cannot be represented by volcanic rocks. The parental melts of the studied melilitite-carbonatite melts probably formed via low-degree partial melting of modally metasomatized continental lithosphere.

1. Introduction

Continental rift systems and to a lesser extent oceanic hotspots impinging on lithosphere >100 km thick typically produce alkali-rich, undersaturated silicate magmas (Le Bas, 1980; Schmidt and Weidendorfer, 2018). The commencement of the rifting process is usually accompanied by a low-volume magma stage characterized by primitive silica-undersaturated melts, such as melilitites or nephelinites (e.g., Dasgupta et al., 2013). These melts form via relatively low degree partial melting at high pressure (p) in the lithospheric upper mantle (about 27–30 kbar, Brey, 1978), with significant CO_2 in their source (up to 5 wt%, Brey, 1978; Dasgupta et al., 2007; Tappe et al., 2007). The latter enhances the probability of subsequent carbonatite melt exsolution from the evolving melilitites and nephelinites (Guzmics et al., 2012; Lee

* Corresponding author.
E-mail addresses: berkesi.marta@epss.hu (M. Berkesi), justine1@gamma.ttk.pte.hu (J.L. Myovela), greg.yaxley@anu.edu.au (G.M. Yaxley), tibor.guzmics@gmail.com (T. Guzmics).

https://doi.org/10.1016/j.gca.2023.03.027
0016-7037/

and Wyllie, 1998). Even though they are less voluminous than alkali basalts at higher degree of partial melting during later stages of rifting, intracratonic melilititic melts are potential parental melts of silicate-carbonatite immiscible liquids. Silicate-carbonatite immiscibility is a crucial process that precedes the crystallization of most carbonatites on the planet (Yaxley et al., 2022). Carbonatite melts are not preserved in the geological record (Guzmics et al., 2011; Weidendorfer et al., 2017), therefore melt compositions and the processes of silicate-carbonatite liquid immiscibility can only be inferred from (1) experimental (e.g., Anenburg et al., 2020; Brooker and Kjarsgaard, 2011; Lee and Wyllie, 1997, 1998; Weidendorfer et al., 2017) and (2) melt inclusion studies (e.g., Berkesi et al., 2020; Guzmics et al., 2019; Mitchell 2009; Panina and Stoppa 2009; Potter et al 2017; Seifert and Thomas, 1995; Sharygin et al., 2012; Solovova et al., 2006; Veksler and Lentz, 2006).

Iron-titanium oxides are common liquidus mineral phases in SiO_2-undersaturated magmas related to carbonatite petrogenesis (Veksler and Teptelev, 1990; Veksler, et al., 1998; Guzmics et al., 2012). Owing to its early crystallization, perovskite ($CaTiO_3$) not only can form accumulations at plutonic depths in the magma chamber, but also it can entrap a high number of the melt droplets from which it crystallized. Perovskite is known to be an excellent host for melt inclusions, due to its stability both mechanically and chemically, allowing high temperature quenching experiments without decrepitation (Guzmics et al., 2012; Nielsen et al., 1997), although contamination effects on isotopic compositions may occur (Tappe and Simonetti, 2012).

In this study, we aim to better understand early-stage melilititic silicate-carbonatite liquid immiscibility at high p and T by the investigation of primary melt inclusions hosted in perovskite-bearing cumulates from Kerimasi volcano in east Africa. The study area (East African Rift System-EARS) is a recent continental rift system and igneous rocks from Kerimasi, and other volcanoes indicate silicate-carbonatite immiscibility. Based on experimental results and field observations, previous melt inclusion studies indicated melilititic compositions for parent melts before immiscibility at the rifting environment of circum-cratonic lithosphere (Church, 1995; Dawson, 2008). Melilitite melts form in the upper mantle (peridotite source rock) through low degree partial melting and require CO_2 (or carbonate) in the source (Alibert et al., 1983; Brey, 1978; Green, 2015; Ivanikov et al., 1998; Foley and Pintér, 2018; Keller et al., 2006; Wilson et al., 1995; Yaxley et al., 2022). This detailed melt inclusion study demonstrates high p-T conditions for the silicate-carbonatite liquid immiscibility in the studied rock. We clarify the compositional characteristics of the parental liquid which may enhance or preclude the occurrence of immiscibility. Finally, we compare the origin of our studied melilitite melt (and conjugate carbonatite) composition with continental intraplate melilitite and nephelinite volcanic rocks and discuss the implications for their formation conditions.

2. Geological setting

The East African Rift System (EARS) is an active rift zone which is generally considered as the classical example of a continental rift system. Formation of the EARS started in the northern part of Africa (Afro-Arabian Dome) during Miocene and then propagated to the south. Along the southward direction, the EARS is divided into two branches, namely the eastern and western rifts. The former is also known as the Gregory Rift and is situated at the boundary between the thick and stable Tanzania Craton and the thinner and more elastic Mozambique Orogenic belt (Dawson, 2008). The Tanzania Craton separates the western rift and Gregory rift of the EARS.

With some rare exceptions, volcanoes of northern Tanzania surround and overlie the metamorphic basements of the Mozambique Orogenic belt. The Gregory Rift is associated with older and younger volcanic products (Guest, 1953), where the extrusive silicate rocks of the younger volcanic products, including the study area (Oldoinyo Lengai, Kerimasi, Meru and Hanang), are characterized by alkaline rocks, i.e., nephelinites and phonolites (Dawson, 2008; Guest, 1953). Alkaline and silica-undersaturated magmas, such as melilitites and nephelinites are common in the Earth's continents and, frequently associated with carbonatites (Fig. 1). They occur typically (1) at the propagating tip and (2) on the flanks of the rift (Williams, 1982). Along the rift zone, the within-rift sequences show a decrease in silica undersaturation with time and the melt composition upon the further progress of the rifting becomes silica-saturated at the rift axes (Macdonald, 2003).

Plutonic rocks in the southern part of the Gregory Rift include ijolite, carbonatite and pyroxenite, occurring as blocks or bombs in pyroclastic tuffs (Dawson, 2008).

Kerimasi is an extinct stratovolcano which last erupted between about 1.1–0.4 Ma ago (Hay, 1976; Macintyre et al., 1974). It is located in eastern part of Gregory Rift valley in northern Tanzania, about 12 km away from Oldoinyo Lengai (OL). OL is Earth's only active carbonatite volcano that periodically erupts natrocarbonatite melts in contrast to all other carbonatite rocks in the geological record which are calcite and dolomite rich (Hay, 1983).

Church (1995) proposed that the primitive magma of Kerimasi volcano was olivine nephelinite, which underwent fractional crystallization and cumulus processes (Dawson et al., 1995; Dawson, 2008). According to Dawson (2008), the primary magma of Kerimasi volcano produced cumulate rocks such as ijolite. In addition, Kerimasi volcano has extrusive and intrusive silicate rocks with the latter occurring as xenoliths (Church, 1995). Intrusive rocks of Kerimasi volcano are mainly ijolite, pyroxenite, uncompahgrite, afrikandite and calcite carbonatite (Church, 1995; Guzmics et al., 2011, 2012; Káldos et al., 2015).

3. Sampling and methods

We collected 15 magnetite-perovskite cumulate rock samples in 2016 from southeast slopes of Kerimasi Volcano, Tanzania. The rocks occurred as xenoliths 5–8 cm in size, embedded in volcanic tuff with a typically iridescent blue color. Petrographic study was conducted using a Nikon ECLIPSE LV100 polarization microscope equipped with Nikon DS-Fi1 camera. For a detailed melt inclusion study, one representative xenolith was chosen. Perovskite grains ($n \sim 150$) were handpicked from the rock for subsequent furnace experiments.

Heating-quenching experiments were conducted using a Carl-Zeiss Jena high temperature (1 atm) furnace, based on the procedures described by Guzmics et al. (2012), to reproduce the trapped melt phases. Temperatures used in the experimental runs were 1050 °C and 1100 °C with an uncertainty of ±20 degrees Celsius. The heating rate was 20–30 degrees Celsius/min. Heated perovskites with their melt inclusions were then quenched with a rate of 300–350 °C/s. Al_2O_3 polishing powder−oil suspension was used to expose the quenched melt inclusions for SEM-EDS analyses. After exposure, the perovskites and their melt inclusions were immersed in oil to prevent alteration of carbonatite melts by the humid air.

In order to obtain the major element composition of the rock-forming minerals and quenched melt phases (Figs. 2 and 3), a Quantax75 EDS-SDD in combination with a Hitachi TM4000Plus microscope was used at the Faculty of Science Research and Instrument Core Facility of Eötvös University, Budapest (ELTE FS-RICF). The beam current for melt and mineral analyses was 200 pA and 2nA, respectively, with 15 kV acceleration voltage. Oil was

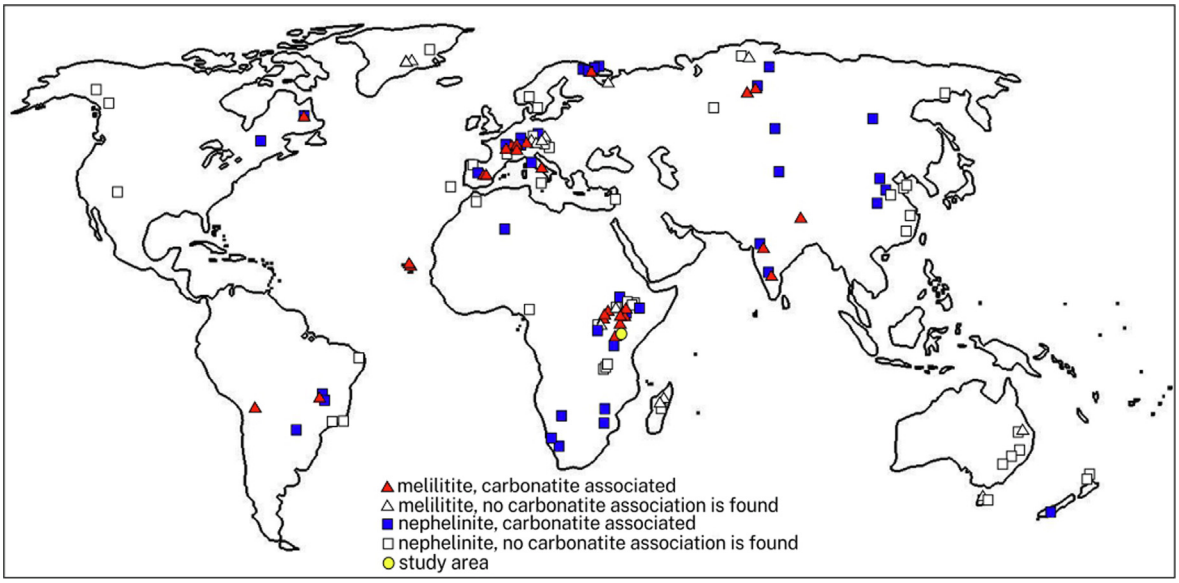

Fig. 1. World map showing the location of the study area (yellow circle – Kerimasi) and the locations of continental melilitite (red triangle) and nephelinite (blue square) volcanic rocks, which are associated with carbonatites (blue squares, red triangles and yellow circles). Empty symbols (square and triangle) indicate only silicate rocks (melilitite or nephelinite) on the location, where no information is available about any associated carbonatite rock. (For interpretation of the references to color in this figure legend, the reader is referred to the web version of this article.)

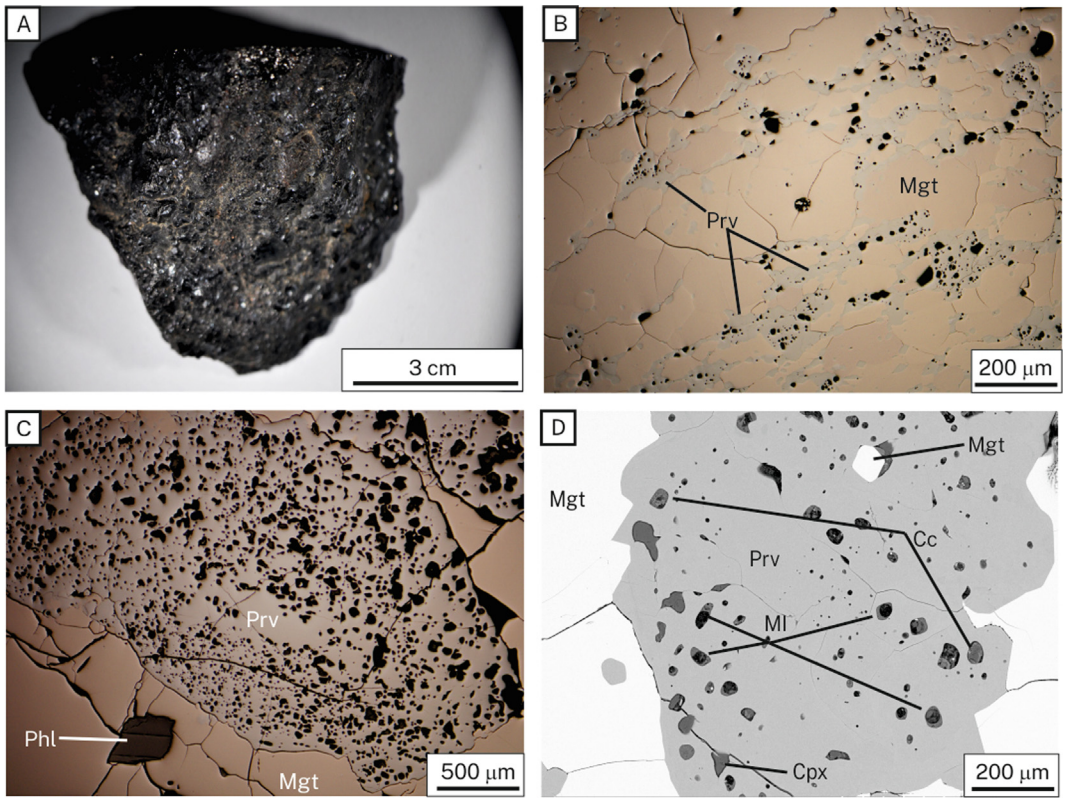

Fig. 2. Representative macro-and microscopic view of the melt inclusions and their enclosing rocks. (A) Stereomicroscopic image showing a typical appearance of the rocks studied, B-C reflected light view; (B) shows the cumulate structure of the selected rock with major magnetite (Mgt) and the melt-inclusion (MI)-hosted in perovskite (Prv) as rock forming minerals. (C) shows the high abundance and primary character of the unheated melt inclusions from core to rim, as well as minor phlogopite. (D) back-scattered electron image showing the unheated inclusions in perovskite, including magnetite, calcite (Cc) and clinopyroxene (Cpx), co-entrapped with the melt inclusions. Phl-phlogopite.

removed from the grains using a soft tissue right before analyses of melt inclusions without using water. Duplicate measurements on the quenched melt phases did not show compositional variation, which indicates no Na vaporization during the analyses. Natural and synthetic standards were used for instrument calibration, and ZAF corrections were applied.

Raman spectroscopy was carried out at the Research and Industrial Relation Center of the Faculty of Science, Eötvös University

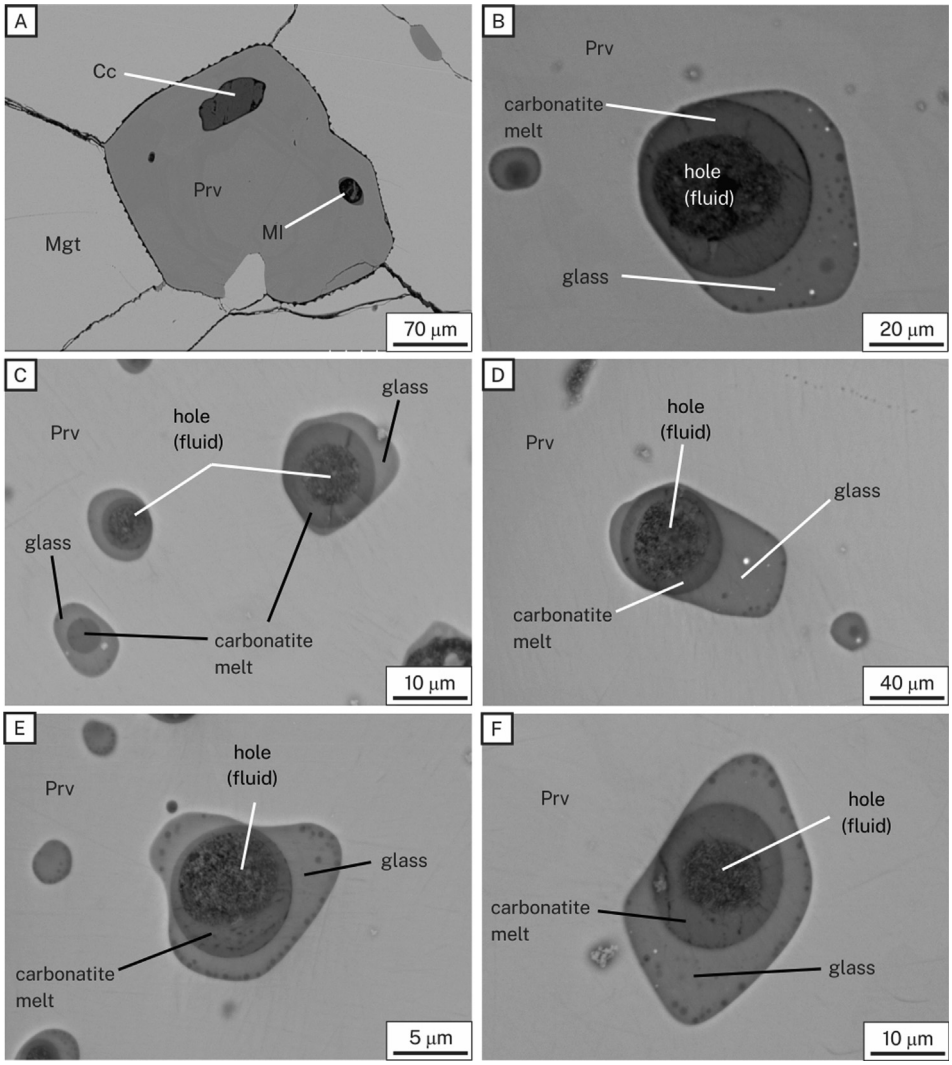

Fig. 3. Back-scattered electron images of perovskite (Prv)-hosted exposed melt inclusions (MI) (A) Image of a perovskite then entrapped melt inclusion and calcite in the same crystal growth zone. Unheated sample. (B-F) Exposed and heated-quenched melt inclusions (run 1100 °C) showing immiscible melilitite (represented by glass) and carbonatite melts. The wide relative volume percentages of glass, quenched carbonatite melt and holes (represent a former fluid phase) show the coexistence of these phases at entrapment.

(ELTE-FS-RICF), Budapest. The measurements were taken using confocal HORIBA Labram HR (800 mm) microspectrometer equipped with Nd-YAG laser with 532 nm excitation wavelength, 1800 grooves/mm optical grating and the width of the confocal pinhole used was 50–200 μm. During the measurements, the acquisition time was 5–50 s using objectives of 10x, 50x and 100x. The lateral size of the laser spot was 1.2 μm, depth of resolution was 1.7 μm using 50 μm size confocal hole and 100x objective. The laser power at the source and surface were 130 mW and approximately 50 mW, respectively. The analysis was conducted with a spectral resolution of 0.7 cm^{-1} at 1398.5 cm^{-1} which was the full width at half maximum of one neon line. Dissolved CO_2-concentrations in the quenched silicate melts were calculated using the method of Morizet et al. (2013).

4. Petrography

4.1. Host rock

The collected rock samples have cumulate textures (Fig. 2a-b) and consist of massive magnetite (~60–80 vol%) and randomly distributed perovskite (~20–35 vol%). Phlogopite, calcite and clinopyroxene constitute less than 5 vol% (Fig. 2b-c). The majority of perovskites are subhedral to euhedral (40–3000 μm). All euhedral perovskites are rich in melt inclusions from core to rim (Fig. 2c-d). Phlogopite and clinopyroxene are subhedral to anhedral (30–1100 μm) and evenly distributed in the rocks (Fig. 2c).

4.2. Melt and mineral inclusions

Unheated perovskite-hosted melt inclusions are both irregular and negative crystal shaped, and are randomly distributed within the crystals (Fig. 2b-d). We therefore interpret them to be primary. The size of the melt inclusions varies from 5 to 100 μm. The silicate melt phase inside the inclusions is glassy, whereas the carbonatite melt phase consists of crystal-aggregates of carbonates. Daughter minerals are calcite, apatite, nyerereite and minor sulfates in the carbonatite (Fig. 5b). Micrometer sized daughter minerals of clinopyroxene often occur in the silicate glass. Perovskite hosts calcite, clinopyroxene and magnetite mineral inclusions (Fig. 2d). Fig. 3 shows the perovskite-hosted melt inclusions after quenching. Run products at 1050 and 1100 °C are (1) silicate melt (quenched as glass), (2) carbonatite melt (quenched as sub-micron crystallized assemblage), and (3) holes representing a

former fluid phase that was lost during melt inclusion exposure. Carbonatite melt typically forms a rounded droplet shape and is surrounded by silicate melt (Fig. 3b-f). The contact between these melts is clearly a meniscus, indicating immiscible melt phases at the run temperatures. The quenched silicate melt, carbonatite melt and holes (fluid) in the perovskite-hosted melt inclusions have shown wide range of their volume proportions. At 1050 °C, the quenched melt inclusions often contained calcite and clinopyroxene that were not completely dissolved into the melts during experiment. At 1100 °C, we detected that all daughter minerals were dissolved into the melts. Nonetheless, calcite, clinopyroxene and magnetite still existed as mineral inclusions in 1100 °C run.

5. Major element geochemistry

5.1. Rock forming minerals

Tables 1 and 2 show the compositions of rock-forming minerals. Magnetite (Table 1a) has uniform composition (all in wt%) of FeO^T (75.0–76.3). It is TiO_2-rich (11.7–12.2), moderate in MgO (3.5–4.0) and Al_2O_3 (2.7–4.1) and low in Cr_2O_3 (<0.1). Based on end-member calculations, it is a solid solution of (all in mole %) magnetite (Fe_3O_4, 42.3–44.7), ulvöspinel (Fe_2TiO_4, 32.2–33.4), magnesioferrite ($MgFe_2O_4$, 12.0–15.0), spinel ($MgAl_2O_4$, 5.7–8.8), jacobsite ($MnFe_2O_4$, 1.7–2.5) and chromite ($CrFe_2O_4$, <1.2). Perovskite has a nearly stochiometric composition of $CaTiO_3$ (Table 1b) with minor contents (all in wt%) of FeO^T (<2.7), Na_2O (0.3–0.7), Nb_2O_5 (0.4–1.8), SrO (up to 0.4), MnO (≤0.3) and Al_2O_3 (≤0.3). Mica is phlogopite with uniform composition (Table 2a) of (all in wt%) MgO (18.7–19.7), Al_2O_3 (15.5–17.0) and K_2O (8.7–9.5). It is moderate in FeO^T (10.1–12.1) and TiO_2 (2.4–3.5) and contains minor Na_2O (0.8–1.1); F and Cl were not detected. Phlogopite H_2O content was calculated to be 4.0–4.1 wt% (Table 2a). Phlogopite shows elevated Al-content (2.7–2.8 atoms per formula unit when normalized to 22 oxygens) balancing the Si-deficit in the tetrahedral position, compared to phlogopites in ijolites and nephelinites (Dawson and Smith, 1992; Sekisova et al., 2015). Clinopyroxene is rich in diopside component (Table 2b) with CaO and MgO content of 23.0–23.9 and 12.3–14.7 wt%, respectively. Besides, it has moderate Al_2O_3-content (3.1–6.1 wt%); in contrast to its low Cr_2O_3-content (up to 0.3 wt%). CaO-content of calcite varies between 52.1 and 54.7 wt%, with SrO content between 0.7 and 3.1 wt% (Table S1).

5.2. Composition of heated-quenched perovskite-hosted melt inclusions

Table 3 shows the composition of coexisting silicate and carbonatite melts (appearing in the same melt inclusions); all silicate glass and quenched carbonate melt compositions are summarized in Table S2 and S3. In general, FeO^T and Al_2O_3 mostly concentrates in silicate melt, whereas CaO is mainly in the carbonatite melt. Therefore, negative correlation on plots of FeO^T vs Al_2O_3, and positive on CaO vs FeO^T in the silicate glass indicates minimal contamination of the carbonatite melt in the silicate melt compositions (Figure S1). A significant characteristic of silicate melts is the very low (all in wt%) SiO_2 (29.4–33.5, Fig. 4) and the high CaO (16.3–24.4) contents (Table 3 and S2). On the total alkali – silica (TAS) diagram, they plot in the foidite compositional field (Fig. 4). In addition, silicate melts are elevated in Na_2O (6.8–12.7), K_2O (1.8–3.2), FeO^T (9.0–13.5), moderate in Al_2O_3 (5.6–10.4), TiO_2 (2.2–3.8), MgO (4.0–5.9) and P_2O_5 (1.0–1.7). Peralkalinity index [$(Na_2O + K_2O)/Al_2O_3$, molar] ranges between 1.7 and 3.3; whereas mg# [$MgO/(MgO + FeO^T)$, molar] varies between 35.1 and 52.5. Carbonatite melts are high in (all in wt%) CaO (28.4–39.0), moderate-to-high in Na_2O (8.2–20.2) + K_2O (4.1–6.6) compositions (total alkalis ranges between 13.1 and 24.3), P_2O_5 (3.0–5.7) and low in FeO^T (0.7–2.6), SiO_2 (1.2–2.9), MgO (1.0–2.6), but moderate in Cl (≤2.3), F (≤1.8), BaO (≤0.9) and SrO (≤0.9) (Table 3 and S3).

Silicate glass in both unheated and heated-quenched melt inclusions were analyzed to determine the effect of possible H_2O loss (e.g., Bakker and Jansen, 1994) during furnace experiments (Fig. 3). Interestingly, no Raman band of H_2O in glass was detected either in unheated or in heated-quenched inclusions, which certainly indicates no or very low water-contents (below detection). For comparison, Guzmics et al. (2019), using the same instrument and parameters revealed H_2O-contents as low as 0.02 wt% in silicate glass. We can therefore state that silicate glass in our melt inclusions contains <0.02 wt%. In addition, the H_2O -poor characteristic of unheated melt inclusions proves that H_2O has not been lost during heating experiments, therefore, and can be treated as indicative of the original H_2O -content of the silicate melt at entrapment. CO_2–content varies between 6.0–9.8 wt% and 5.4–9.1 wt% in the unheated and heated-quenched silicate glasses, respectively (Table 3, Fig. 5a).

6. Discussion

6.1. Origin of the magnetite-perovskite cumulates

Magnetite-perovskite cumulates are known to form potential Fe-Ti ores that can be related to dunites, clinopyroxenites, carbonatites and kimberlites (Potter et al., 2018). Although Knipping et al. (2019) have recently revealed a model including magnetite floating along with degassing H_2O-rich fluid bubbles and reaching the upper part of the magma chamber, this scenario in our case is unlikely, as degassing fluid compositions are expected to be rather CO_2-rich (Guzmics et al., 2019) instead of aqueous. We rather propose that the main driving force of the accumulation of magnetite and perovskite, owing to the high density of these oxide minerals relative to the magma and rock-forming silicate minerals, was gravitational settling to the bottom of the magma chamber of the investigated rock. The high abundance of primary melt inclusions enclosed in the perovskites (Fig. 3b-f) indicates that this mineral

Table 1a
Composition of magnetite, Kerimasi magnetite-perovskite cumulate, Tanzania (wt%).

No.	1	2	3	4	5	6	7	8	9	10	11	12	13	14	15	16
TiO_2	12.0	12.0	12.1	12.0	12.2	12.2	12.1	12.1	12.1	11.8	12.0	12.0	12.1	12.1	11.7	12.0
Al_2O_3	3.2	3.1	3.1	4.1	3.1	2.9	3.2	3.3	3.0	3.0	3.0	2.8	2.7	2.8	2.9	2.9
Cr_2O_3	<0.1	<0.1	<0.1	<0.1	<0.1	<0.1	<0.1	<0.1	<0.1	<0.1	<0.1	<0.1	<0.1	<0.1	<0.1	<0.1
V_2O_3	0.3	0.4	0.1	0.0	0.3	0.3	0.1	<0.1	<0.1	0.2	<0.1	0.3	<0.1	0.3	<0.1	0.2
FeO^T	75.3	75.3	75.5	75.0	75.2	75.8	75.4	75.3	75.5	76.0	75.9	76.0	76.3	75.9	76.3	76.2
MnO	0.7	0.7	0.6	0.5	0.6	0.6	0.6	0.6	0.7	0.8	0.6	0.6	0.5	0.6	0.7	0.6
MgO	3.9	3.9	4.0	3.8	4.0	3.7	4.0	3.9	3.9	3.6	3.7	3.7	3.6	3.7	3.6	3.5
Total	95.4	95.4	95.3	95.5	95.4	95.4	95.3	95.2	95.2	95.4	95.2	95.4	95.2	95.4	95.2	95.4

FeO^T - all Fe expressed as FeO.

Table 1b
Composition of perovskite, Kerimasi magnetite-perovskite cumulate, Tanzania (wt%).

No.	1	2	3	4	5	6	7	8	9	10	11	12	13	14	15	16
TiO_2	54.5	54.2	56.2	56.2	56.3	57.1	55.0	55.9	56.6	55.7	56.8	56.9	57.0	55.8	57.0	55.0
Al_2O_3	<0.1	0.2	0.2	0.3	0.3	0.2	<0.1	0.2	0.2	0.2	0.3	0.3	0.3	0.2	0.2	0.3
FeO^T	2.6	2.7	1.5	1.5	1.3	1.1	1.3	0.9	1.2	1.1	1.2	1.0	1.1	1.3	1.7	1.5
MnO	<0.1	<0.1	<0.1	<0.1	<0.1	<0.1	0.3	<0.1	<0.1	<0.1	<0.1	<0.1	<0.1	<0.1	<0.1	<0.1
SrO	0.2	0.3	0.2	0.2	0.2	<0.1	0.3	0.3	0.3	0.2	0.2	0.2	0.4	0.2	0.3	0.3
CaO	37.5	36.9	38.9	38.3	38.1	39.2	38.1	37.9	38.6	38.3	38.2	38.4	38.7	38.3	38.1	38.0
Na_2O	0.6	0.7	0.3	0.4	0.5	0.3	0.3	0.4	0.4	0.5	0.4	0.5	0.4	0.4	0.5	0.3
Nb_2O_5	0.8	1.8	0.4	0.8	0.5	0.8	0.5	0.6	0.9	0.7	0.5	0.6	0.8	0.7	0.7	0.6
Total	96.3	96.7	97.6	97.7	97.2	98.7	95.7	96.1	98.2	96.7	97.7	97.8	98.7	96.9	98.5	95.8

Table 2a
Composition of phlogopite, Kerimasi magnetite-perovskite cumulate, Tanzania (wt%).

No.	1	2	3	4	5	6	7	8	9	10	11	12	13	14	15	16
SiO_2	36.1	35.6	35.8	35.0	35.8	36.2	35.8	35.7	35.9	35.7	36.3	36.2	35.5	35.4	36.0	35.8
TiO_2	2.4	3.5	3.0	3.5	3.1	3.4	2.9	2.7	2.9	3.0	2.7	3.0	3.1	3.5	3.0	3.2
Al_2O_3	16.4	16.4	16.0	15.7	16.0	15.8	16.1	17.0	16.0	16.0	16.3	16.1	15.9	15.5	15.9	15.7
FeO^T	10.3	10.9	11.1	11.6	10.9	11.1	10.8	10.1	10.8	10.7	10.5	10.9	11.1	12.1	10.7	11.3
MnO	<0.1	<0.1	<0.1	0.3	<0.1	0.2	0.2	0.4	0.2	0.2	0.2	0.2	0.2	<0.1	<0.1	<0.1
MgO	19.6	19.4	19.2	18.9	19.2	18.7	19.3	19.7	19.2	19.1	19.5	18.8	19.0	18.7	19.2	18.8
CaO	0.2	<0.1	<0.1	0.2	0.2	<0.1	<0.1	<0.1	<0.1	<0.1	<0.1	<0.1	<0.1	<0.1	<0.1	<0.1
BaO	1.1	0.2	0.6	0.7	0.6	0.8	1.0	0.5	0.6	0.9	0.6	0.6	0.8	0.6	0.8	0.8
Na_2O	1.0	0.9	1.0	0.8	1.1	0.9	1.0	0.9	0.9	0.9	1.0	0.9	0.9	0.8	0.9	0.9
K_2O	8.9	8.9	8.9	9.0	8.7	8.9	9.0	8.7	9.4	9.4	8.8	9.2	9.1	9.3	9.5	9.3
Total	96.0	95.9	95.8	95.7	95.7	96.0	95.9	95.7	96.0	95.9	95.9	95.9	95.8	96.1	96.1	95.9
Mw (H_2O)	4.1	4.1	4.1	4.0	4.1	4.1	4.1	4.1	4.1	4.1	4.1	4.1	4.1	4.0	4.1	4.1

Mw (H_2O) - calculated H_2O content.

Table 2b
Composition of clinopyroxene. Kerimasi magnetite-perovskite cumulate. Tanzania (wt%).

No.	1	2	3	4	5	6	7	8	9	10	11	12
SiO_2	47.2	46.3	46.8	46.3	47.5	47.1	49.1	48.3	49.3	47.4	50.4	47.1
TiO_2	2.5	2.4	2.4	2.7	2.3	2.6	1.9	2.0	1.8	2.6	1.7	2.4
Al_2O_3	5.6	5.9	5.7	6.1	4.8	5.8	4.0	4.5	3.8	5.8	3.1	5.8
Cr_2O_3	0.3	<0.1	<0.1	0.3	0.2	<0.1	0.2	<0.1	0.2	<0.1	<0.1	<0.1
FeO^T	7.3	7.6	7.6	7.8	7.0	7.5	6.4	6.6	6.0	7.2	5.5	7.3
MnO	<0.1	<0.1	0.2	<0.1	<0.1	<0.1	0.2	0.2	<0.1	<0.1	0.2	0.2
MgO	12.9	12.3	12.6	12.3	13.1	12.5	13.7	13.8	14.2	13.0	14.7	12.9
CaO	23.0	23.5	23.2	23.2	23.9	23.2	23.6	23.8	23.6	23.1	23.7	23.0
Na_2O	0.7	0.8	0.7	0.7	0.5	0.7	0.5	0.5	0.6	0.6	0.5	0.7
Total	99.5	98.8	99.1	99.2	99.3	99.4	99.6	99.5	99.3	99.6	99.6	99.3

FeO^T all Fe expressed as FeO.

was a liquidus phase with no visible evidence of secondary textural changes. The random occurrence of magnetite, calcite and clinopyroxene crystal inclusions co-entrapped with melt inclusions in perovskite (Fig. 2d) indicate the co-crystallization of these mineral phases. The relatively high temperature (~1100 °C) of the dissolution of daughter minerals in perovskites-hosted melt inclusions also supports their early crystallization. Heated-quenched perovskite-hosted melt inclusions (Fig. 3) contain immiscible silicate and carbonatite melts together with a fluid phase in highly variable proportions. This phase-proportional characteristic clearly shows the presence of fluid-saturated and immiscible silicate-carbonatite melts during precipitation of perovskites studied, as has been described in previous papers (Guzmics et al., 2012; Káldos et al., 2015; Sekisova et al., 2015).

6.2. Liquid immiscibility in silicate-carbonatite petrogenesis

Three quarters of global carbonatite rocks are spatially and temporally associated with alkaline silicate rocks, such as melilitites, nephelinites and syenites (Yaxley et al., 2022), which indicates that silicate-carbonatite liquid immiscibility is a basic formation mechanism of most carbonatite rocks. The overwhelming majority are calcite carbonatites (Weidendorfer et al., 2017; Wei et al., 2020). Therefore, understanding silicate-carbonatite immiscibility together with the formation of $CaCO_3$-rich carbonatite melts (able to precipitate voluminous calcite) is crucial to deciphering where and how the calcite carbonatites derive and evolve.

The low SiO_2 together with high carbonate and alkali contents in silicate melts are thought to be key factors enabling intersection of a silicate-carbonatite two-liquid field (Yaxley et al., 2022 and references therein). For example, Schmidt and Weidendorfer (2018) showed that the only two known oceanic islands (Cape Verde and the Canary Islands) with carbonatites, contain associated primitive basanites with the lowest SiO_2 (38–42 wt%) and highest total alkalis (4–5 wt%) within 17 oceanic islands worldwide. These two oceanic islands are underpinned by the thickest lithospheres, resulting in an increase of p of melt formation that further enhances the CO_2 solubility in silicate melts. All these factors increase the chance for immiscibility, that has also been experimentally proven using oceanic volcanic rocks as starting material (Weidendorfer and Asimow, 2022). However, we show below that in intracontinental settings especially in rift zones, the primitive melt compositions, the p

Table 3a
Composition of coexisting immiscible silicate (silm) and carbonatite (cbm) melts in perovskite-hosted melt inclusions quenched after heating to 1050 °C, Kerimasi magnetite-perovskite cumulate, Tanzania (wt%).

1050 °C	silm2_1	cbm2_1	silm5_1	cbm4_2	silm5_2	cbm4_1	silm9_1	cbm5_1	silm9_2	cbm5_2	silm10_1	cbm6_1
SiO_2	30.9	2.4	31.1	1.9	32.2	2.9	33.3	2.2	32.1	2.4	31.2	2.5
TiO_2	3.5	0.3	2.5	0.3	2.6	0.3	2.9	0.3	2.4	0.3	2.8	0.4
Al_2O_3	8.7	n.d.	9.8	n.d.	9.7	n.d.	10.2	n.d.	9.8	n.d.	10.2	n.d.
FeO^T	13.3	1.0	9.3	0.9	10.1	2.0	9.4	1.2	10.5	1.5	9.3	1.2
MnO	0.2	<0.1	<0.1	<0.1	0.2	<0.1	0.2	<0.1	0.2	n.d.	0.2	0.2
MgO	4.2	2.1	5.2	2.1	5.4	2.6	5.0	2.1	4.5	2.1	5.4	1.6
SrO	n.d.	0.5	0.2	0.7	<0.1	0.8	n.d.	0.9	0.3	0.6	n.d.	0.2
CaO	21.9	30.7	18.9	29.3	20.1	29.1	19.4	32.3	19.2	33.1	17.4	29.5
BaO	0.2	0.3	0.6	0.5	0.6	n.d.	0.4	n.d.	0.2	0.3	0.2	n.d.
Na_2O	8.1	17.5	11.3	18.8	9.7	17.3	9.9	15.7	10.2	14.3	12.7	17.8
K_2O	2.6	4.1	2.0	4.5	1.8	4.2	2.3	4.5	2.3	4.6	1.9	6.1
P_2O_5	1.2	4.3	1.1	3.8	1.4	4.4	1.5	5.0	1.2	4.8	1.1	3.9
F	0.2	0.3	0.3	0.8	0.3	0.7	0.4	0.8	0.3	0.4	0.2	0.3
SO_3	1.1	n.d.	1.2	<0.1	1.5	0.2	0.8	n.d.	1.3	n.d.	0.7	2.6
Cl	0.2	0.3	<0.1	0.8	<0.1	0.7	<0.1	1.1	0.2	1.0	<0.1	2.3
Total	96.3	63.8	93.7	64.5	95.7	65.2	95.7	66.0	94.6	65.6	93.4	68.4
CO_2 calculated		36.2		35.6		34.8		34.1		34.5		31.6
$Na_2O + K_2O$	10.7	21.6	13.3	23.3	11.5	21.5	12.2	20.2	12.4	18.9	14.6	23.9
PI	1.8		2.1		1.8		1.8		2.0		2.3	
mg#	35.7		49.9		49.0		48.8		43.4		50.7	

Table 3b
Composition of coexisting immiscible silicate (silm) and carbonatite (cbm) melts in perovskite-hosted melt inclusions quenched after heating to 1100 °C, Kerimasi magnetite-perovskite cumulate, Tanzania (wt%).

1100 °C	silm1_2	cbm1_1	silm2	cbm8	silm5	cbm11	silm7	cbm21	silm8	cbm24
SiO_2	29.9	2.4	31.0	2.4	31.4	2.1	30.7	1.4	29.5	1.9
TiO_2	3.8	0.5	3.4	0.5	3.8	0.5	3.4	0.5	3.1	0.5
Al_2O_3	8.1	n.d.	7.6	n.d.	9.5	n.d.	8.5	n.d.	7.8	n.d.
FeO^T	12.5	2.0	10.9	1.9	11.1	2.4	11.3	1.5	13.5	2.2
MnO	0.2	n.d.	0.2	n.d.	0.3	n.d.	0.3	n.d.	0.4	n.d.
MgO	4.6	1.2	5.6	2.5	5.0	1.6	4.7	1.3	4.6	1.2
SrO	n.d.	0.7	0.2	0.7	0.2	0.9	n.d.	0.8	<0.1	0.4
CaO	24.2	39.0	20.9	33.3	21.3	32.1	22.5	32.7	24.4	37.8
BaO	0.2	n.d.	0.5	0.2	n.d.	0.5	n.d.	<0.1	0.5	0.9
Na_2O	7.3	8.2	9.5	13.1	9.0	14.0	8.1	15.3	6.8	10.3
K_2O	2.6	4.9	2.1	4.8	2.1	4.8	2.4	5.5	2.6	4.6
P_2O_5	1.2	3.9	1.6	4.2	1.2	3.5	1.1	5.5	1.3	3.0
F	<0.1	0.2	0.4	1.5	0.2	0.2	0.3	0.8	0.3	1.8
SO_3	1.0	0.3	1.2	0.4	1.5	0.8	1.0	0.2	0.8	n.d.
Cl	<0.1	0.9	<0.1	0.2	0.2	0.5	<0.1	0.3	0.2	1.0
Total	95.7	64.1	95.3	65.8	96.6	63.8	94.4	65.9	95.5	65.6
CO_2 calculated		36.0		34.2		63.8		34.1		34.4
CO_2 analyzed	9.1									
$Na_2O + K_2O$	9.9	13.1	11.6	17.9	11.1	18.8	10.5	20.7	9.4	14.9
PI	1.8		2.4		1.8		1.9		1.8	
mg#	39.5		47.8		44.5		42.7		37.6	

PI - peralkalinity index = $(Na_2O + K_2O)/Al_2O_3$ molar, mg# - $MgO/(MgO + FeO^T)$ molar, n.d.-not detected, CO_2 calculated represents difference to 100, CO_2 analyzed represents data calculated from Raman analyzes.

and T of immiscibility are generally different from those considered in oceanic settings. The 29–34 wt% SiO_2-content of the perovskite-hosted silicate melts (Table 3, Table S2) indicates extreme silica undersaturation, accompanied by high carbonate- (5.4–9.1 wt%), total-alkali- (8.5–15.9 wt%, where Na_2O = 6.7–12.7 wt% K_2O = 1.8–3.2 wt%) and medium MgO- (4.0–5.9 wt%) contents (Table S2). These silicate melts can be defined as CaO-rich (16.3–24.3 wt%) and mafic, larnite-normative melilitite because their normative compositions include high melilite and lesser larnite, olivine, perovskite, nepheline and diopside. Similar melilite-normative, sodium-rich melts are characteristically formed through low-degree partial melting of mantle (1–3%, Green, 2015 and their references therein) at relatively high p (≥3 GPa, Yaxley et al., 2022, Baudouin and Parat, 2020). Besides, experimental works discovered that low-degree partial melting of upper mantle peridotites at around 2–3 GPa produces melilitite melts only when there is significant amount of CO_2 (and subsequently H_2O) in the source (Brey, 1978; Foley and Pintér, 2018). Pintér et al. (2021) demonstrated that incipient melt in upper mantle peridotites is CO_2-rich. CO_2 solubility in melilitite melts, generally increases with increasing p, achieving a concentration of ~9 wt% at 3 GPa (Brey and Green, 1976). Carbon-dioxide, once it dissolves into the low-silica melt, will form CO_3^{2-} anions (Ni and Keppler, 2013; Moussallam et al., 2016). This is also evidenced in studied melilitite melts showing 5–9 wt% dissolved CO_2 (Table S2, Fig. 5a), which can be explained by their formation at high p (~2–3 GPa). The composition of the melilitite melt (Table 3, S2) however, is undoubtedly different from that of the intracontinental melilitites and nephelinites, based on 146 melilitite and 640 nephelinite volcanic rock data, using the GEOROC (https://georoc.mpch-mainz.gwdg.de/Georoc/) database

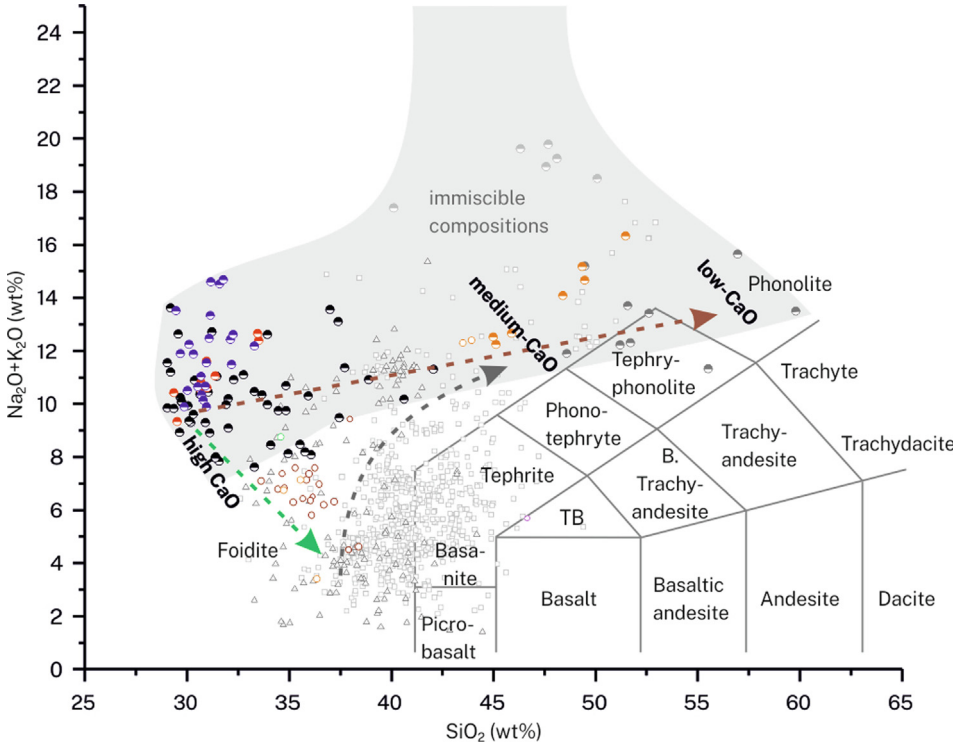

Fig. 4. Total alkalis – silica (TAS) diagram showing the silicate glass, representing the melilitite melt composition, in the melt inclusions quenched at 1050 °C (purple half-filled circles) and 1100 °C (red half-filled circles). For comparisons, silicate glass in melt inclusions from plutonic melilite (heated to 1050 °C, Guzmics et al., 2012) are plotted as black half-filled circles. Note that any half-filled circles represent silicate melt compositions from coexisting immiscible silicate-carbonatite melts. Light grey half-filled circles: silicate melt compositions from experimental run product at 850 °C and 0.5 GPa (Kjarsgaard et al., 1995), dark grey half-filled circles: melt inclusion-hosted silicate glass data from a volcanic, evolved nephelinite-phonolite at Kerimasi (850 °C, Guzmics et al., 2019). Empty triangles and squares represent melilitite and nephelinite volcanic rocks, respectively, from continental settings (based on GEOROC database, https://georoc.mpch-mainz.gwdg.de/Georoc/). Silicate melt compositions from melt inclusions (with no compositional data for coexisting immiscible carbonatite melt) are plotted from Elbe Zone (in plutonic melilitite at 1150 °C, Seifert and Thomas, 1995), from Gardiner complex (in plutonic melilitite at 1050–1100 °C, Nielsen et al., 1997), from Mt. Vulture (in volcanic trachy-basalt at 1250 °C, Panina and Stoppa, 2009). These silicate melts data are indicated by open circles with rim colors of green, brown and purple, respectively. Experimental data are from Cape Verde (from basanite to phonolite, 1100–1250 °C, Weidendorfer and Asimow, 2022) are indicated by orange circles. Grey area indicates a compositional range of natural silicate liquids immiscible with carbonatite melts. Green dashed arrow shows the direction of an initially low-degree high-CaO partial melt towards increasing degree of partial melting from the same source (e.g., deep continental lithosphere). Grey dashed arrow indicates the schematic evolutionary trend of primitive highly magnesian melilitite and nephelinite melts (during fractional crystallization) to immiscibility. Brown dashed arrow shows the evolutional path of silicate melts that coexist with an immiscible carbonatite melt from high (1100 °C) to low (850 °C) temperatures. TB – trachybasalt, B. Trachy-andesite – basaltic trachy-andesite. (For interpretation of the references to color in this figure legend, the reader is referred to the web version of this article.)

(Figs. 4 and 6). After our selection procedure (see Supplementary Material), these rocks are thought to be representative of melts with small contributions of cumulate minerals. Figs. 4 and 6 show that the overwhelming majority of melilitite and nephelinite volcanic rocks have higher MgO + FeO^T contents accompanying higher mg# (up to 0.77) and much lower CaO and alkali contents than the melilitite melts in our melt inclusions (mg# = 0.35–0.52). In addition, no other melilitite and nephelinite rocks are as strongly SiO_2-undersaturated as the studied melilitite melts (Fig. 4). The question therefore arises at what conditions can silicate-carbonatite immiscibility for these distinct compositions be predicted?

6.3. CaO- versus MgO-rich systems

We plotted our melt data together with experimentally determined silicate-carbonatite two-liquid fields in the pseudoternary systems SiO_2 + Al_2O_3 + TiO_2 — CaO — Na_2O — CO_2 (Brooker and Kjarsgaard, 2011) and SiO_2 + Al_2O_3 + TiO_2 — MgO + FeO^T — Na_2O + K_2O — CO_2 (Lee and Wyllie, 1997, 1998) on Fig. 6a and b, respectively. Comparison of pseudoternary systems offers a demonstration of how the size of the two-liquid field depends on CaO/(MgO + FeO^T), p and T (Fig. 6). A petrologically important phenomenon we should note is when immiscible silicate-carbonatite melts are in equilibrium with clinopyroxene and calcite on the liquidus. This is identical when the silicate-calcite liquidus field boundary surface reaches the immiscibility field and, therefore, defines points 'f' and 'g' (see Fig. 6a) in the system SiO_2 + Al_2O_3 + TiO_2 — CaO — Na_2O + K_2O (Lee and Wyllie, 1996, 1997, 1998). In our samples the coexistence of the silicate-carbonatite melts with calcite and clinopyroxene, at melt entrapment, is evidenced petrographically (Fig. 2d). Based on above experimental works, we estimated the silicate-calcite liquidus surface at various p, shown with black dashed curves on Fig. 6a. At high p (≥1 GPa) the silicate-calcite liquidus surface terminates at the two-liquid field at points 'f' and 'g' very close to the composition of our immiscible melts quenched from 1100 °C (Fig. 6a). At lower p (~0.5 GPa) points 'f' and 'g' join at the thermal maximum of the two-liquid field far away from any known natural melt compositions (Fig. 6a). At p of ~ 0.2 GPa silicate-calcite liquidus surface does not likely touch any experimentally confirmed two-liquid fields in the system SiO_2 + Al_2O_3 + TiO_2 — CaO — Na_2O + K_2O (Fig. 6a) (Kjarsgaard, 1998; Lee and Wyllie, 1998).

In addition, natural, low degree mantle-derived melts contain significant amounts of MgO and FeO^T, so a combined interpretation of CaO- (Fig. 6a) and MgO + FeO^T-bearing (Fig. 6b) systems is important. In the CaO-bearing system (Fig. 6a), as the p increases, the immiscibility field expands, while temperature has the

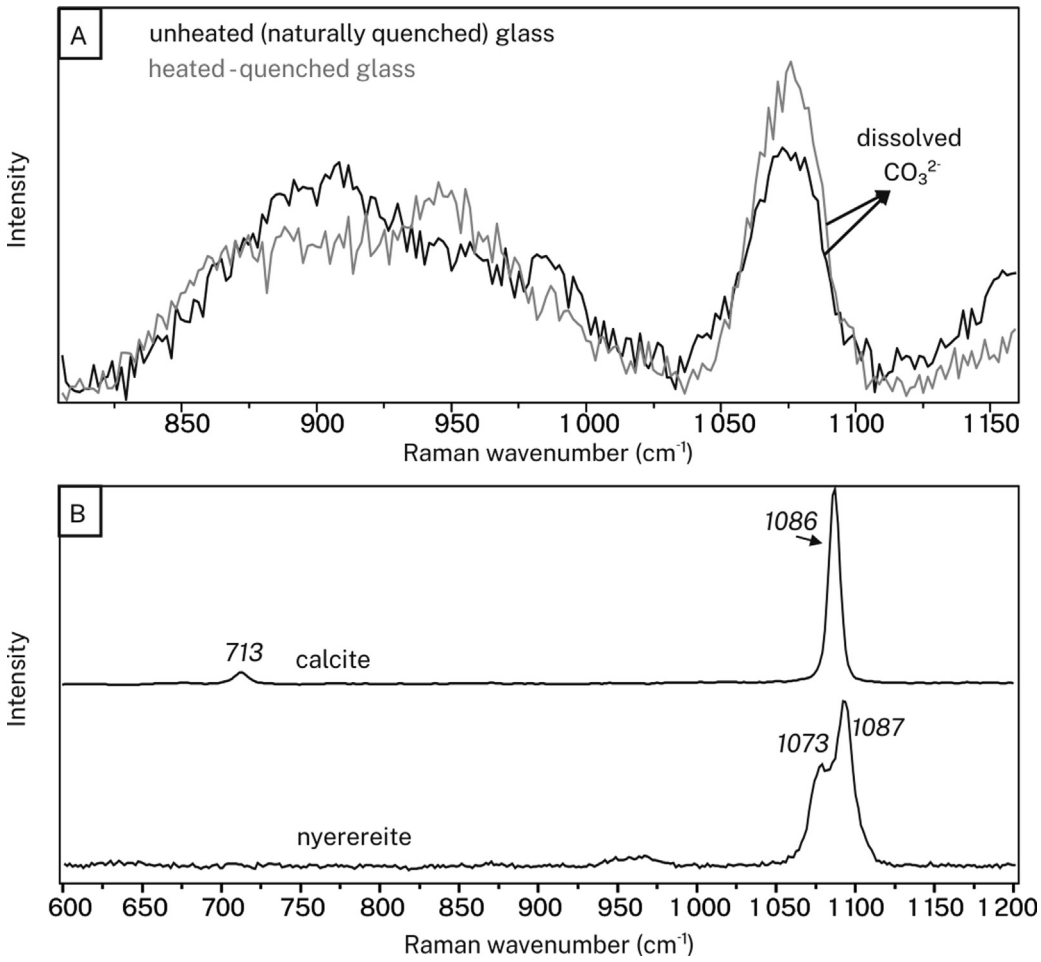

Fig. 5. (A) Representative Raman spectra on both unheated and heated-quenched (run 1100 °C) silicate glasses. Besides the typical envelope-shaped characteristics, the bands related to high intensity and thus high concentration of dissolved carbonate is demonstrated here (CO_2 contents are 7.5 and 8.0 wt% in unheated and heated-quenched melt inclusions, respectively). Also, given the small intensity difference between and heated-quenched and unheated glasses it can be stated that likely there was no H_2O-loss from the silicate glasses due to the furnace experiments. (B) Representative Raman spectra of carbonate (calcite and nyerereite) daughter minerals in the unheated melt inclusions.

opposite effect. Considering a minimum temperature of 1050 °C for primitive alkaline silicate melts (Guzmics et al., 2012), the two-liquid field determined at 1.5 GPa and 1275 °C (Brooker and Kjarsgaard, 2011) is a good approximation for its maximum extent (Fig. 6a). In contrast, an increase in temperature and especially p in a Mg + Fe-bearing system results in more pronounced reduction of the two-liquid field (Fig. 6b). Thus, at high p (≥1 GPa), the addition of mafic components (FeO^T and MgO) to the CaO-bearing system causes increased shrinkage of the two-liquid field. This strongly limits the composition of Mg + Fe-rich silicate melts capable of exsolution of carbonatite melts at high p (≥1 GPa) and T (≥1050-1100 °C). The composition of the studied CaO-rich and mafic melilitite melts in Fig. 6a is well within the 1.5 GPa immiscibility field. In Fig. 6b, they are outside the field determined at 1 GPa, close to the limbs. This arrangement allows silicate melts with similar compositions to those reported here to exsolve carbonatite melts at a p of 1 to 1.5 GPa. The compositions of the studied carbonatite melts plot close to the limb of 1.5 GPa field (Fig. 6a), also supporting high-p immiscibility.

6.4. Potential of silicate melts to exsolve $CaCO_3$-rich carbonatite melts in high proportion

Compositions of magnesian melilitites and nephelinites are far away from immiscibility field at any reasonable pressures (Fig. 6). Figs. 4 and 6 suggest that prolonged fractional crystallization may lead initially magnesian silicate melts to reach the two-liquid field only at lower T (<~850–900 °C) and unmix alkali-rich carbonatite melts. At this point the silicate melts show phono-tephrite–tephri-phonolite compositions and are likely to have lost most of their original MgO and CaO contents (Figs. 4 and 6). Kjarsgaard (1998) studied experimentally immiscible melilitite-carbonatite melts at 0.5 GPa and 0.2 GPa and showed carbonatite melts exsolved below 1025 °C and 930 °C, respectively. Although these immiscible melts can precipitate calcite after crystallization of liquidus minerals (silicates and oxides) at temperatures <925 °C (0.5 GPa) and <900 °C (0.2 GPa), calcite is certainly not a liquidus phase (Lee and Wyllie, 1998). This is also true for experiments using nephelinite starting compositions from oceanic hot spots. Even though the immiscibility is observed at somewhat higher p and T i.e., 1 GPa and 1100 °C (Weidendorfer and Asimow, 2022), immiscible silicate melts compositions are strongly reduced in CaO (<10.50 wt%), MgO (<1.85 wt%) and FeO^T (<3.58 wt%) relative to our CaO-rich and mafic melilitite melts (Table 3) and far from calcite liquidus surface at 1 GPa (Fig. 6a).

Melt inclusions (this study, Guzmics et al., 2012, 2019; Nielsen et al., 1997) and further experimental studies (Kjarsgaard et al., 1995; Brooker and Kjarsgaard, 2011) show that the lower the temperature the lower the $CaCO_3$ content of the immiscible carbonatite melt (Fig. 6a). Fractionated and evolved silicate melts such as phonolites or evolved nephelinites are enriched in alkalis and decreased in divalent cations as Ca and Mg and are not able to dis-

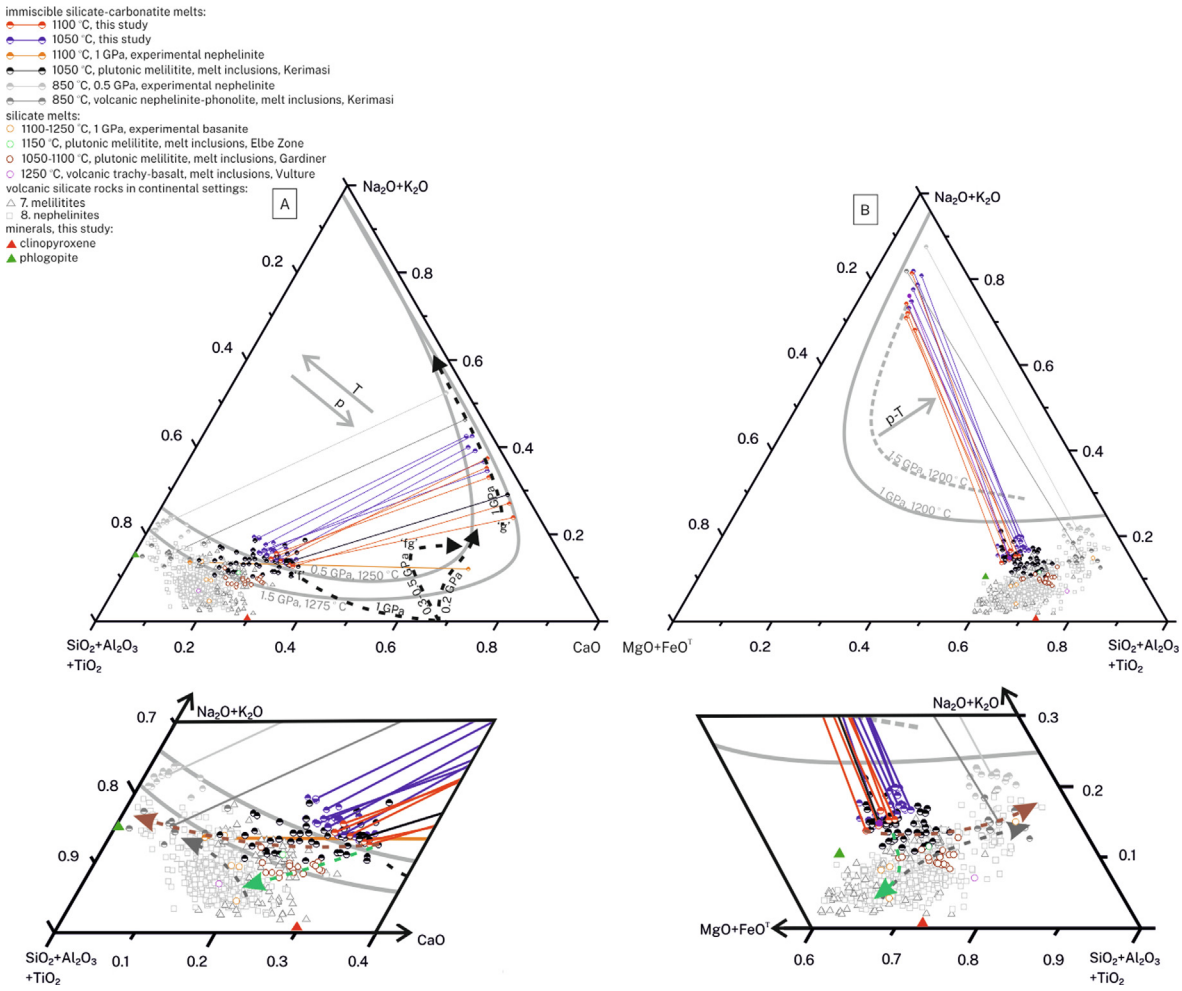

Fig. 6. (A) SiO_2 + Al_2O_3 + TiO_2 – CaO – Na_2O + K_2O pseudoternary and (B) SiO_2 + Al_2O_3 + TiO_2 – MgO + FeO^T – Na_2O + K_2O pseudoternary diagrams (projected from CO_2) and their close-up view (parallelograms) showing the main compositional factors of high p – high T silicate-carbonatite liquid immiscibility. Arrows and melt compositional data are the same as in the Fig. 4 and thus are explained in there. Grey solvii (both continuous and dashed ones) show the extension of the silicate-carbonatite melt immiscibility field at different p and T, after the experimental works of Lee and Wyllie, 1998 and Brooker and Kjarsgaard, 2011. Grey solid arrows labeled as p and/or T indicates the direction of shape change of the immiscibility with changing p and T. Red, blue and grey lines indicate tie-lines, which connect the immiscible melt compositions. Black dashed curves demonstrate the calcite liquidus curve at different p. Points of 'f' and 'g' define when the silicate-calcite liquidus field boundary surface reaches the immiscibility field and, therefore, define coexistence of the silicate-carbonatite melts with calcite and clinopyroxene, at melt entrapment. (For interpretation of the references to color in this figure legend, the reader is referred to the web version of this article.)

solve carbonate ions in such high amounts compared to strongly Si-undersaturated CaO-rich silicate melts with high divalent cation contents. Low p (≤0.5 GPa) and T (≤850 °C) immiscible carbonatite melts are enriched in alkalis, and not as strongly calcite-normative as the high-p-T carbonatite melts. Thus, it can be concluded that the lower the p and T, the lower the chance for calcite precipitation and the silicate melts tend to exsolve a smaller portion of carbonatite melt with increased alkali and decreased CaO contents. A high formation p of the melt inclusions is also suggested by the calcite + cpx daughter mineral phase assemblage and the absence of any melilite-group mineral (likely akermanite) in the melt inclusions. The lack of akermanite in a melilite-normative melt, like the silicate melt in melt inclusions (Figs. 2 and 3), could be explained by entrapment p conditions higher than the akermanite stability in the presence of a CO_2-rich melt, that can be reached at ≥~0.7 GPa, according to Yoder (1975).

The melilitite melt compositions are clearly proving their potential for reaching immiscibility at 1100 °C as inferred from the heating-quenching experiments. Immiscible carbonatite melts at this T are rich in $CaCO_3$ and elevated in P_2O_5 (3.0–5.3 wt%) (Table 3). Calcite saturation of the melt at such high T and p provides the capability for the carbonate melt to crystallize significant volumes of calcite carbonatite rocks (often composed of calcite and apatite), once it can separate from the silicate melt (Guzmics et al., 2012; Weidendorfer et al., 2017, Yaxley et al., 2022). Our study shows that melt compositions likely provide one of the earliest states of immiscible carbonatite melt that precipitates calcite at high T (≥1100 °C) and thus due to its further evolution, it potentially forms calcite carbonatite rocks much more voluminously, than the Mg-rich melilitites or nephelinites.

6.5. Implication for parental melt composition

In this section, we aim to estimate the composition and understand the formation conditions of the SiO_2-undersaturated melilitite melts represented in the studied melt inclusions, compared to primitive melilitite/nephelinite intracontinental volcanic rocks. Note, neither the studied melt inclusions nor the volcanic rocks likely represent an actual parent melt as their compositions could have been slightly modified by either early fractionation at plutonic depths (e.g., Tappe et al., 2003) or cumulation effect of minerals (Glazner, 1994).

The main driving force for a parent silicate melt to reach an immiscibility field at high-p (~1–1.5 GPa) could have been both the T decrease and crystal fractionation-controlled melt compositional change (Nielsen et al., 1997; Guzmics et al., 2012). The studied melilitite melts and the intracontinental melilite volcanic rocks demonstrate minor compositional shifts due to crystal fractionation from a parent melt. Among the major elements, strong SiO_2-undersaturation (and thus the melilite normative character) is a key point as fractionation trends result in increase in SiO_2 and Al_2O_3, together with a decrease in the mg#, likely reaching compositions of evolved phonolitic melt composition (Figs. 4 and 6). Yet, early magmatic co-fractionation of clinopyroxene and phlogopite might shift from forsterite-saturated melanephelinite melt towards larnite-normative melilitite melt (Veksler et al., 1998) and is theoretically demonstrated by a shift from the SiO_2 + Al_2O_3-rich to the CaO rich-compositions on Fig. 6a. This process, however, is not supported for melilitite-type melts (Fig. 6a) and therefore its effect is unlikely to occur in nature. On the other hand, the crystallization of early cumulate oxides, like magnetite and perovskite, should increase the melt SiO_2-content. Therefore, oxide precipitation was not responsible for production of strong SiO_2-undersaturation in the melilitite melts (Figs. 4 and 6).

The compositional difference between the studied melilitite melts and the intracontinental volcanic rocks (Fig. 6) could be accounted for by different source rocks for the parental melt and/or difference in the extent of partial melting (Fig. 7). Experiments and studies on natural rocks indicate that melilitite rocks, occurring in volcanic fields from continental settings formed by low-degree (~5%, Brey and Green, 1977) partial melting of a garnet lherzolite (Fig. 7) with high CO_2 content (Brey, 1978), sometimes assuming minor phlogopite in the source (e.g., Baudouin and Parat, 2020; Tappe et al., 2007; Wilson et al., 1995).

Garnet lherzolite, however, cannot be considered as a source for the studied melilitite melt even when assuming a lower degree of partial melting (~<1–3 %) than the volcanic counterparts (~<5%). According to experimental observations, silicate melts formed by low-degree partial melts of a CO_2-bearing garnet lherzolite source will be low in SiO_2 (~<30 wt%), high in CO_2 (~<15 wt%), and low in alkalis (2–3 wt%) but quite high in MgO (19–20 wt%) (Dasgupta et al., 2007). As discussed in the previous section, the last two compositional features likely preclude silicate-carbonatite immiscibility (Fig. 6). Generally considering a lherzolite source rock, continuous increase in the degree of partial melting from ~<1% to ~ 10%, melt compositions will show progressive enrichment in MgO and SiO_2 and decrease in CaO-and alkali-content (Frey et al., 1978; Klein and Langmuir, 1987; Dasgupta et al., 2013; Green, 2015). Thus, the increasing degree of partial melting decreases the likelihood of early silicate-carbonatite immiscibility. For example, once the degree of partial melting forms an alkali basaltic melt composition (~8–11 %, Zou and Zindler, 1996), then it will hardly be capable of exsolving carbonatite melt at any stage of its evolution (Fig. 7).

To sum up, the high alkali (9–15 wt%, where Na_2O = 6.7–12.7 wt% K_2O = 1.8–3.2 wt%) and CaO contents (16–24 wt%), and the medium MgO-content (4.0–5.9 wt%) of the studied melilitite melts (Table 3, Table S2) are very unlikely to have resulted from low degree melting of a four-phase (olivine, orthopyroxene, clinopyroxene and garnet) lherzolite source. This statement seems to be valid even in case of near solidus melts of a non-metasomatized garnet lherzolite source as shown experimentally (e.g., Davis et al., 2011), where $Na_2O + K_2O$ cannot reach a value higher than 3–4 wt%. The source of the studied melilitite could rather be an enriched lithospheric segment: either a modally metasomatized lherzolite containing amphiboles and phlogopites or even a MARID-type (acronym for mica-amphibole-rutile-ilmenite-diopside) lithospheric segment (Fig. 7), to account for the elevated alkalis and CaO-content in the studied silicate glass (Förster et al., 2018). The studied area, Kerimasi, supports this idea as it belongs to the North Tanzanian Volcanic Province, where the underlying lithosphere is inferred to be extremely heterogeneous from a lithological point of view (e.g., Dawson, 2008). Numerous studies point to the assumption that the lower part of the cratonic lithosphere is intensely metasomatized along the rift (Lloyd and Bailey, 1975; Norry et al., 1980; Clement, 1982; Dawson and Smith, 1992; Dawson, 2002; Ngwenya and Tappe, 2021), as indicated by pargasite-bearing rocks along the eastern rift (Foley et al., 2012), and phlogopite-bearing rocks along the eastern rift (Rosenthal et al., 2009; Baudouin and Parat, 2020) as well as seismologic data (Wölbern et al., 2012). Moreover, Dawson (1999) remarked that each xenolith suite in Tanzania contains modally metasomatized xenoliths. This lithospheric environment could have been the source for many fossil carbonatites, forming during intracontinental rifting in the past as well. In numerous locations where fossil carbonatites occur, modally metasomatized mantle xenoliths were brought by the volcanic activity to the surface, which is contemporaneous and cogenetic with the carbonatite rock formations, i.e., Bearpaw (Downes et al., 2004), Kaiserstuhl (Sigmund and Keller, 1994), Kola peninsula (Downes et al., 2005), Vulture volcano (Stoppa et al., 2009), eastern Canada (Tappe et al., 2006). Moreover, Tappe et al. (2008) state that a cold cratonic mantle lithosphere is an important host of MARID-type vein assemblages, derived from preceding tectonic and magmatic events. However, isotopic systematics rather support that modal metasomatism of the deep lithosphere, (possibly by a fluid phase as the metasomatic agent) could be related to the same rifting process that gives the source for the carbonatite-melilitite immiscible melts (Tappe et al., 2017). It all strongly indicates that silicate and carbonatite melts that are represented in the studied melt inclusions could have been formed at intracontinental settings where a modally metasomatized mantle lithosphere produced low degree partial melts and could be one of the key tools to crystallize calcite carbonatite rocks voluminously (Fig. 7).

CaO-enrichment in the source may be derived from melting of pargasitic amphibole, as well as diopsidic clinopyroxene in the source. Additionally, according to previous studies, low-degree partial melts having $Na_2O/K_2O \geq 1$ indicate an assemblage in the source that is richer in amphibole relative to phlogopite (Green, 1973; Foley et al., 1999). In this case, considering the stability of pargasite (Green et al., 2010); the melt could have been formed at a depth not greater than ~90 km (~3 GPa).

6.6. Fe-Ti cumulates as containers of early immiscibility?

The melilitite melt composition reported here is not represented in any volcanic edifices with melilititic and nephelitinic rock compositions, based on the extensive GEOROC database (https://georoc.mpch-mainz.gwdg.de/Georoc/). We can therefore conclude that the melilitite melt in our samples, at this early stage, did not produce volcanic events on the surface (Fig. 7) and consequently might have remained hidden.

This study suggests that oxide cumulates, mainly built up by magnetite and perovskite can thus be a significant container of such early-stage silicate – carbonate melt (+fluid) immiscibility, as the extremely SiO_2-undersaturated melts would preferentially crystallize oxides besides minor silicate and carbonate minerals at their early stage of melt evolution. Therefore, such cumulate rocks can never be representative of the melt(s) from which they crystallized. Consequently, melt inclusion studies of Fe-Ti cumulates related to alkaline magmatism could be a key tool to understand early magmatic processes. It has also been discovered that natural representations of incipient melt compositions from a continental lithosphere at high p can be rather studied via primary

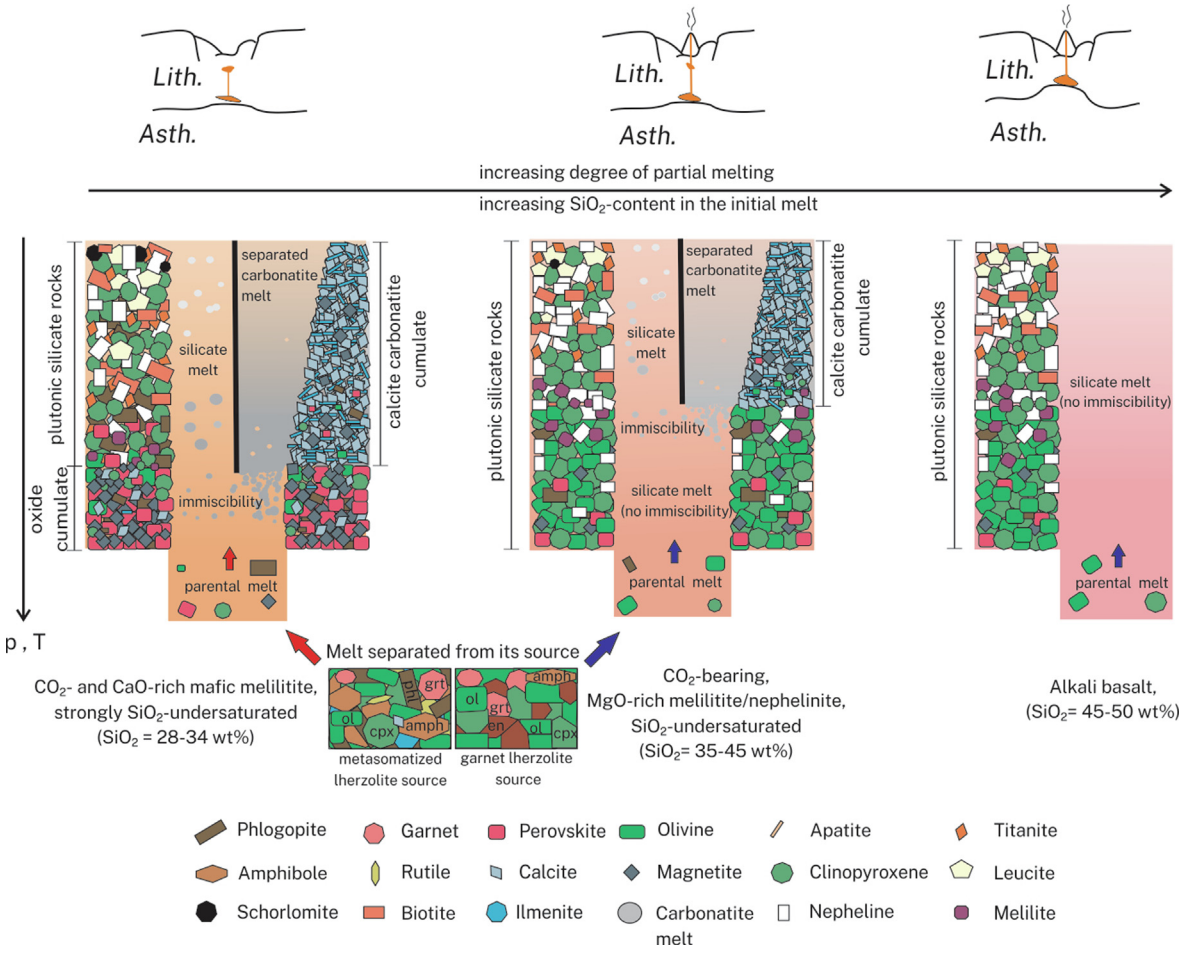

Fig. 7. Schematic figure showing the differing capacity of parental melts to produce calcite-carbonatites. Each schematic column represents the simplified evolution of the different parental melts (evolution direction goes upward as the p and T decreases) and tends to show both the relative p and T where carbonatite melt exsolves (if it happens at all) from the parental melt resulting in silicate-carbonatite immiscibility. In addition, the relative volumes of the crystallizing calcite carbonatite rocks are also indicated (right hand side of the column, if exists), besides the silicate rocks (left hand side of the columns). The different parental melts are formed either by the partial melting of presumably different source rock (deep lithosphere) and/or via different degrees of melting. Moreover, on top of the columns, we demonstrate the formation of these parental melts in different stages of rifting. The studied melt inclusions represent the left side column, the continental melilitite and nephelinite volcanic rocks are represented by the middle column, whereas the right-side column indicates a parental melt that likely formed by higher degree partial melting than the two other columns and thus is not capable to exsolve any carbonatite melts. Our finding is that the CaO- and alkali-rich CO_2-bearing SiO_2-undersaturated melt is the most capable melt to reach the immiscibility at higher p (~ ≥1 GPa) and higher T (~1100 °C), relative to a CaO- and alkali-poorer but MgO-richer but also CO_2-bearing SiO_2-undersaturated melt, which will produce silicate-carbonatite-immiscibility at lower p. For details, see text.

melt inclusions hosted by oxide-rich cumulates instead of any volcanic rocks.

7. Conclusions

Perovskite-hosted melt inclusions from Kerimasi volcano demonstrate the existence of immiscible melilitite and carbonatite melts (+fluid phase) at high p (≥1 GPa) and high T (≥1050 °C) during entrapment. Compositions of these immiscible melts have been compared to melilitite and primitive nephelinite volcanic rock compositions, all from an intracontinental setting, and the following conclusions can be drawn. Carbonatite melt is CaO and alkali-rich whereas melilitite melt is mafic, strongly SiO_2-undersaturated and rich in CaO-, CO_2- and alkalis. These melts are represented in the studied melt inclusions but not in the melilitite and primitive nephelinite volcanic rocks in the geological record. The source of the parent melt of the melt inclusions is most probably modally metasomatized deep lithospheric mantle, which is likely more enriched in pargasite than in phlogopite. The parent melt is inferred to have formed by low degree partial melting of such a source.

However, melts formed from high degrees of partial melting of this source, or any melt from a non-metasomatized deep lithospheric source (i.e., garnet lherzolite), will have a significant MgO content. This is a compositional feature of most continental melilitite and primitive nephelinite volcanic rocks. The relatively high MgO precludes early high p-T immiscibility; this will be delayed until much more evolved stages of melt evolution are reached. In contrast, CaO and alkali-rich melilitite melt, formed at the onset of continental rifting, bear significantly higher potential to form volumetrically significant calcite carbonatite rocks than their more magnesian, alkali-rich counterparts.

Declaration of Competing Interest

The authors declare that they have no known competing financial interests or personal relationships that could have appeared to influence the work reported in this paper.

Acknowledgements

M. Berkesi and T. Guzmics were supported by the research project provided by the National Research Development and Innova-

tion Office of Hungary, project number: NKFIH_K 142855. J. L. Myovela is thankful to the Doctoral School of Earth Sciences, University of Pécs for its support in this research. This is the 118th publication of the Lithosphere Fluid Research Lab.

Appendix A. Supplementary material

It includes one figure showing the Al_2O_3 versus FeO^T and CaO versus FeO^T diagrams of the silicate glasses within the melt inclusions. In addition, there is a description of the selection rules used for the GEOROC database on melilitites and primitive nephelinites. Tables show the entire dataset for major element composition of calcite (Table S1), silicate glasses (melts) and quenched carbonatite melts (Table S2 and S3, respectively). Supplementary data to this article can be found online at https://doi.org/10.1016/j.gca.2023.03.027.

References

Alibert, C., Michard, A., Albarède, F., 1983. The transition from alkali basalts to kimberlites: Isotope and trace element evidence from melilitites. Contrib. Mineral. Petrol. 82, 176–186.

Anenburg, M., Mavrogenes, J.A., Frigo, C., Wall, F., 2020. Rare earth element mobility in and around carbonatites controlled by sodium, potassium, and silica. Sci. Adv. 6, eabb6570.

Bakker, R.J., Jansen, J.B.H., 1994. A mechanism for preferential H_2O leakage from fluid inclusions in quartz, based on TEM observations. Contrib. Mineral. Petrol. 116, 7–20.

Baudouin, C., Parat, F., 2020. Phlogopite-olivine nephelinites erupted during early stage rifting, North Tanzanian Divergence. Front. Earth Sci. 8, 277.

Berkesi, M., Bali, E., Bodnar, R.J.B., Szabó, Á., Guzmics, T., 2020. Carbonatite and highly peralkaline nephelinite melts from Oldoinyo Lengai Volcano, Tanzania: The role of natrite-normative fluid degassing. Gondwana Res. 85, 76–83.

Brey, G., 1978. Origin of olivine melilitites – chemical and experimental constraints. J. Volcanol. Geotherm. Res. 3, 61–88.

Brey, G.P., Green, D.H., 1976. Solubility of CO_2 in olivine melilitite at high pressures and role of CO_2 in the Earth's upper mantle. Contrib. Mineral. Petrol. 55, 217–230.

Brey, G., Green, D.H., 1977. Systematic study of liquidus phase relations in olivine melilitite + H_2O + CO_2 at high pressures and petrogenesis of an olivine melilitite magma. Contrib. Mineral. Petrol. 61, 141–162.

Brooker, R.A., Kjarsgaard, B.A., 2011. Silicate–carbonate liquid immiscibility and phase relations in the system SiO_2–Na_2O–Al_2O_3–CaO–CO_2 at 0,1–2,5 GPa with applications to carbonatite genesis. J. Petrol. 52, 1281–1305.

Church, A.A., 1995. The petrology of the Kerimasi carbonatite volcano and the carbonatites of Oldoinyo Lengai with a review of other occurrences of extrusive carbonatite. Ph.D. thesis, University College, London, U.K.

Clement, C.R., 1982. A comparative geological study of some major kimberlite pipes in the Northern Cape and Orange Free State, Ph.D. thesis (2 vols.), University of Cape Town.

Dasgupta, R., Hirschmann, M.M., Smith, N.D., 2007. Partial melting experiments of peridotite + CO_2 at 3 GPa and genesis of alkalic ocean island basalts. J. Petrol. 48, 2093–2124.

Dasgupta, R., Mallik, A., Tsuno, K., Withers, A.C., Hirth, G., Hirschmann, M.M., 2013. Carbon-dioxide-rich silicate melt in the Earth's upper mantle. Nature 493, 211–215.

Davis, F.A., Hirschmann, M.M., Humayun, M., 2011. The composition of the incipient partial melt of garnet peridotite at 3GPa and the origin of OIB. Earth Planet. Sci. Lett. 308, 380–390.

Dawson, J.B., 2002. Metasomatism and partial melting in upper-mantle peridotite xenoliths from the Lashaine volcano, northern Tanzania. J. Petrol. 43, 1749–1777.

Dawson, J.B., 2008. The Gregory rift valley and Neogene-recent volcanoes of northern Tanzania. Geological Society Memoir No.33, London.

Dawson, J.B., Smith, J.V., 1992. Olivine-mica pyroxenite xenoliths from northern Tanzania: metasomatic products of upper-mantle peridotite. J. Volcanol. Geotherm. Res. 50, 131–142.

Dawson, J.B., Smith, J.V., Steele, I.M., 1995. Petrology and mineral chemistry of plutonic igneous xenoliths from the carbonatite volcano, Oldoinyo Lengai, Tanzania. J. Petrol. 36, 797–826.

Dawson, J.B., 1999. Melting and metasomatism in spinel peridotite xenoliths from Labait, Tanzania. In: Gurney, J.J., Pascoe, M.D., Richardson, S.H. (Eds.), Proceedings of the 7th International Kimberlite Conference, Red Roof Design, Cape Town, pp. 164–173.

Downes, H., Macdonald, R., Upton, B.G.J., Cox, K.G., Bodinier, J.-L., Mason, P.R.D., James, D., Hill, P.G., Hearn Jr., B.C., 2004. Ultramafic xenoliths from the Bearpaw Mountains, Montana, USA: evidence for multiple metasomatic events in the lithospheric mantle beneath the Wyoming Craton. J. Petrol. 45, 1631–1662.

Downes, H., Elena Balaganskaya, E., Beard, A., Liferovich, R., Demaiffe, D., 2005. Petrogenetic processes in the ultramafic, alkaline and carbonatitic magmatism in the Kola Alkaline Province: A review. Lithos 85, 48–75.

Foley, S.F., Pintér, Zs., 2018. Primary melt compositions in the Earth's mantle. In: Kono, Y., Sanloup, C. (Eds.), Magmas Under Pressure, Advances in High-Pressure Experiments on Structure and Properties of Melts. Elsevier, Netherlands, pp. 3–42.

Foley, S.F., Musselwhite, D.S., van der Laan, S.R., 1999. Melt Compositions from ultramafic vein assemblages in the lithospheric mantle: a comparison of cratonic and non-cratonic settings. In: Gurney, J.J. (Ed.), Proceedings of the 7th International Kimberlite Conference -J.B. Dawson volume, Red Roof, Cape Town, pp. 238–246.

Foley, S.F., Link, K., Tiberindwa, J.V., Barifaijo, E., 2012. Patterns and origin of igneous activity around the Tanzanian craton. J. African Earth Sci. 62, 1–18.

Förster, M.W., Prelević, D., Schmück, H.R., Buhre, S., Marschall, H.R., Mertz-Kraus, R., Jacob, D.E., 2018. Melting phlogopite-rich MARID: Lamproites and the role of alkalis in olivine-liquid Ni-partitioning. Chem. Geol. 476, 429–440.

Frey, F.A., Green, D.H., Roy, S.D., 1978. Integrated models of basalt petrogenesis: a study of quartz tholeiites to olivine melilitites from southeastern Australia utilizing geochemical and experimental petrological data. J. Petrol. 19, 463–513.

Glazner, A.F., 1994. Foundering of mafic plutons and density stratification of continental crust. Geology 22, 435–438.

Green, D.H., 2015. Experimental petrology of peridotites, including effects of water and carbon on melting in the Earth's upper mantle. Phys. Chem. Minerals 42, 95–122.

Green, D.H., Hibberson, W.O., Kovács, I., Rosenthal, A., 2010. Water and its influence on the lithosphere–asthenosphere boundary. Nature 467, 448–451.

Green, D.H., 1973. Experimental studies on a model upper mantle composition at high pressure under water-saturated and water-undersaturated conditions. Earth Planet. Sci. Lett. 19, 37–53.

Guest, N.J., 1953. The geology and petrology of the Engaruka - Oldoinyo Lengai - Lake natron area of northern Tanganyika territory. PhD thesis, University of Sheffield.

Guzmics, T., Berkesi, M., Bodnar, R.J., Fall., A., Bali, E., Milke, R., Vetlényi, E., Szabó, Cs., 2019. Natrocarbonatites: A hidden product of three-phase immiscibility. Geology 47, 527–530.

Guzmics, T., Mitchell, R.H., Szabó, C.s., Berkesi, M., Milke, R., Abart, R., 2011. Carbonatite melt inclusions in coexisting magnetite, apatite and monticellite in Kerimasi calciocarbonatite, Tanzania: melt evolution and petrogenesis. Contrib. Mineral. Petrol. 161, 177–196.

Guzmics, T., Mitchell, R.H., Szabó, C.s., Berkesi, M., Milke, R., Ratter, K., 2012. Liquid immiscibility between silicate, carbonate and sulfide melts in melt inclusions hosted in co-precipitated minerals from Kerimasi volcano (Tanzania): evolution of carbonated nephelinitic magma. Contrib. Mineral. Petrol. 164, 101–122.

Hay, R.L., 1976. Geology of the Olduvai Gorge: A study of sedimentation in a semiarid basin. Ph.D. thesis. University of California Press, Berkeley, pp.203.

Hay, R.L., 1983. Natrocarbonatite tephra of Kerimasi volcano, Tanzania. Geology 11, 599–602.

Ivanikov, V.V., Rukhlov, A.S., Bell, K., 1998. Magmatic evolution of the melilitite–carbonatite–nephelinite dyke series of the Turiy Peninsula (Kandalaksha Bay, White Sea, Russia). J. Petrol. 39, 2043–2059.

Káldos, R., Guzmics, T., Mitchell, R.H., Dawson, J.B., Milke, R., Szabó, C., 2015. A melt evolution model for Kerimasi volcano, Tanzania: Evidence from carbonate melt inclusions in jacupirangite. Lithos 238, 101–119.

Keller, J., Zaitsev, A.N., Wiedenmann, D., 2006. Primary magmas at Oldoinyo Lengai: The role of olivine melilitites. Lithos 91, 150–172.

Kjarsgaard, B.A., 1998. Phase relations of a Carbonated High-CaO Nephelinite at 0.2 and 0.5 GPa. J. Petrol. 39, 2061–2075.

Kjarsgaard, B.A., Hamilton, D.L., Peterson, T.D., 1995. Peralkaline nephelinite/carbonatite liquid immiscibility: comparison of phase compositions in experiments and natural lavas from Oldoinyo Lengai. In: Bell, K., Keller, J. (Eds.), Carbonatite Volcanism: Oldoinyo Lengai and the Petrogenesis of Natrocarbonatites. IAVCEI Proceedings in Volcanology 4. Springer-Verlag, Berlin, pp. 163–190.

Klein, E.M., Langmuir, C.H., 1987. Global correlations of ocean ridge basalt chemistry with axial depth and crustal thickness. J. Geophys. Res. 92, 8089–8115.

Knipping, J.L., Webster, J.D., Simon, A.C., Holtz, S., 2019. Accumulation of magnetite by flotation on bubbles during decompression of silicate magma. Sci. Rep. 9, 3852.

Le Bas, M.J., 1980. Alkaline magmatism and uplift of continental crust. Proc. Geol. Assoc. 91, 33–38.

Lee, W.-J., Wyllie, P.J., 1996. Liquid Immiscibility in the Join $NaAlSi_3O_8$-$CaCO_3$ to 2–5 GPa and the origin of calciocarbonatite magmas. J. Petrol. 37, 1125–1132.

Lee, W.-J., Wyllie, P.J., 1997. Liquid immiscibility between nephelinite and carbonatite from 2.5 to 1.0 GPa compared with mantle melt compositions. Contrib. Mineral Petrol. 127, 1–16.

Lee, W.-J., Wyllie, P.J., 1998. Petrogenesis of carbonatite magmas from mantle to crust, constrained by the system CaO–(MgO+FeO*)–(Na_2O+K_2O)–(SiO_2+Al_2O_3+TiO_2)–CO_2. J. Petrol. 39, 495–517.

Lloyd, F.E., Bailey, D.K., 1975. Light element metasomatism of the continental mantle: the evidence and the consequences. Phys. Chem. Earth 9, 389–416.

Macdonald, R., 2003. Magmatism of the Kenya Rift Valley: a review. Trans. Royal Soc. Edinburgh: Earth Sci. 93, 239–253.

Macintyre, R.M., Mitchell, J.G., Dawson, B.J., 1974. Age of fault movements in Tanzanian Sector of East African Rift System. Nature 247, 354–356.

Mitchell, R.H., 2009. Peralkaline nephelinite–natrocarbonatite immiscibility and carbonatite assimilation at Oldoinyo Lengai, Tanzania. Contrib. Mineral. Petrol. 158, 589–598.
Morizet, Y., Brooker, R.A., Iacono-Marziano, G., Kjarsgaard, B.A., 2013. Quantification of dissolved CO_2 in silicate glasses using micro-Raman spectroscopy. Am. Mineral. 98, 1788–1802.
Moussallam, Y., Florian, P., Corradini, D., Morizet, Y., Sator, N., Vuilleumier, R., Guillot, B., Iacono-Marziano, G., Schmidt, B.C., Gaillard, F., 2016. The molecular structure of melts along the carbonatite–kimberlite–basalt compositional joint: CO_2 and polymerization. Earth Planet. Sci. Lett. 434, 129–140.
Ngwenya, N.S., Tappe, S., 2021. Diamondiferous lamproites of the Luangwa Rift in central Africa and links to remobilized cratonic lithosphere. Chem. Geol. 568, 120019.
Ni, H., Keppler, H., 2013. Carbon in silicate melts. Rev. Mineral. Geochem. 75, 251–287.
Nielsen, T.F.D., Solovova, I.P., Veksler, I.V., 1997. Parental melts of melilitolite and origin of alkaline carbonatite: evidence from crystallised melt inclusions, Gardiner complex. Contrib. Mineral. Petrol. 126, 331–344.
Norry, M.J., Truckle, P.F.I., Lippard, S.J., Hawkesworth, C.J., Weaver, S.D., Marriner, G. F., 1980. Isotope and trace element evidence from lavas, bearing on mantle heterogeneity beneath Kenya. Philos. T. R. Soc. A 297, 259–271.
Panina, L., Stoppa, F., 2009. Silicate-carbonate-salt liquid immiscibility and origin of the sodalite-haüyne rocks: study of melt inclusions in olivine foidite from Vulture volcano. S. Italy Open Geosci. 1, 377–392.
Pintér, Z.s., Foley, S.F., Yaxley, G.M., Rosenthal, A., Rapp, R.P., Lanati, A.W., Rushmer, T., 2021. Experimental investigation of the composition of incipient melts in upper mantle peridotites in the presence of CO_2 and H_2O. Lithos 396–397, 106224.
Potter, N.J., Kamenetsky, V.S., Simonetti, A., Goemann, K., 2017. Different types of liquid immiscibility in carbonatite magmas: A case study of the Oldoinyo Lengai 1993 lava and melt inclusions. Chem. Geol. 455, 376–384.
Potter, N.J., Ferguson, M.R.M., Kamenetsky, V.S., Chakhmouradian, A.R., Sharygin, V. V., Thompson, J.M., Goemann, K., 2018. Textural evolution of perovskite in the Afrikanda alkaline–ultramafic complex, Kola Peninsula, Russia. Contrib. Mineral. Petrol. 173, 100.
Rosenthal, A., Foley, S.F., Pearson, D.G., Nowell, G.M., Tappe, S., 2009. Petrogenesis of strongly alkaline primitive volcanic rocks at the propagating tip of the western branch of the East African Rift. Earth. Planet. Sci. Lett. 284, 236–248.
Schmidt, M.W., Weidendorfer, D., 2018. Carbonatites in oceanic hotspots. Geology 46, 435–438.
Seifert, W., Thomas, R., 1995. Silicate-carbonate immiscibility: A melt inclusion study of olivine melilitite and wehrlite xenoliths in Tephrite from the Elbe Zone, Germany. Chem. Erde 55, 263–279.
Sekisova, V.S., Sharygin, V.V., Zaitsev, A.N., Strekopytov, S., 2015. Liquid immiscibility during crystallization of forsterite-phlogopite ijolites at Oldoinyo Lengai Volcano, Tanzania: Study of melt inclusions. Russian Geol. Geophys. 56, 1717–1737.
Sharygin, V.V., Kamenetsky, V.S., Zaitsev, A.N., Kamenetsky, M.B., 2012. Silicate-natrocarbonatite liquid immiscibility in 1917 eruption combeite-wollastonite nephelinite, Oldoinyo Lengai Volcano, Tanzania: Melt inclusion study. Lithos 152, 23–39.
Sigmund, J., Keller, J., 1994. Amphibole and garnet bearing mantle xenoliths in the Kaiserstuhl, Germany: relation to diatreme and carbonatite. Min. Mag. 58A, 840–841.
Solovova, I.P., Girnis, A.V., Ryabchikov, I.D., Simakin, S.G., 2006. High temperature carbonatite melt and its interrelations with alkaline magmas of the Dunkel'dyk complex, southeastern Pamirs. Doklady Earth Sci. 410, 1148–1151.
Stoppa, F., Jones, A.P., Sharygin, V.V., 2009. Nyerereite from carbonatite rocks at Vulture volcano: implications for mantle metasomatism and petrogenesis of alkali carbonate melts. Cent. Eur. J. Geosci. 1, 131–151.
Tappe, S., Foley, S.F., Kjarsgaard, B.A., Romer, R.L., Heaman, L.M., Stracke, A., 2008. Between carbonatite and lamproite—Diamondiferous Torngat ultramafic lamprophyres formed by carbonate-fluxed melting of cratonic MARID-type metasomes. Geochim. Cosmochim. Acta 72, 3258–3286.
Tappe, S., Foley, S.F., Pearson, D.G., 2003. The Kamafugites of Uganda: a mineralogical and geochemical comparison with their Italian and Brazilian analogues. Per. Mineral. 72, 51–77.
Tappe, S., Foley, S.F., Jenner, G.A., Heaman, L.M., Kjarsgaard, B.A., Romer, R.L., Stracke, A., Joyce, N., Hoefs, J., 2006. Genesis of ultramafic lamprophyres and carbonatites at Aillik Bay, Labrador: a consequence of incipient lithospheric thinning beneath the North Atlantic Craton. J. Petrol. 47, 1261–1315.
Tappe, S., Foley, S.F., Stracke, A., Romer, R.L., Kjarsgaard, B.A., Heaman, L.M., Joyce, N., 2007. Craton reactivation on the Labrador Sea margins: $^{40}Ar/^{39}Ar$ age and Sr–Nd–Hf–Pb isotope constraints from alkaline and carbonatite intrusives. Earth. Planet. Sci. Lett. 256, 433–454.
Tappe, S., Romer, R.L., Stracke, A., Steenfelt, A., Smart, K.A., Muehlenbachs, K., Torsvik, T.H., 2017. Sources and mobility of carbonate melts beneath cratons, with implications for deep carbon cycling, metasomatism and rift initiation. Earth. Planet. Sci. Lett. 466, 152–167.
Tappe, S., Simonetti, S., 2012. Combined U-Pb geochronology and Sr–Nd isotope analysis of the Ice River perovskite standard, with implications for kimberlite and alkaline rock petrogenesis. Chem. Geol. 304–305, 10–17.
Veksler, I.V., Lentz, D.R., 2006. Parental magmas of plutonic carbonatites, carbonate-silicate immiscibility and decarbonation reactions: evidence from melt and fluid inclusions. In: Webster, J.D. (Ed.), Melt Inclusions in Plutonic Rocks-Mineralogical Association of Canada, Short Course 36, Montreal, Quebec, p. 123–149.
Veksler, I.V., Fedorchuk, Y.M., Nielsen, T.F.D., 1998. Phase equilibria in the silica-undersaturated part of the $KAlSiO_4 \pm Mg_2SiO_4 \pm Ca_2SiO_4 \pm SiO_2 \pm F$ system at 1 atm and the larnite-normative trend of melt evolution. Contrib. Mineral. Petrol. 131, 347–363.
Veksler, I.V., Teptelev, M.P., 1990. Conditions for crystallization and concentration of perovskite-type minerals in alkaline magmas. Lithos 26, 177–189.
Wei, C-W., Cheng Xu, C., Chakhmouradian, A.R., Brenna, M., Kynicky, J., Song, W.-L., 2020. Carbon–Strontium Isotope Decoupling in Carbonatites from Caotan (Qinling, China): Implications for the Origin of Calcite Carbonatite in Orogenic Settings. J. Petrol., 61, egaa024.
Weidendorfer, D., Asimow, P.A., 2022. Experimental constraints on truly conjugate alkaline silicate – carbonatite melt pairs. Earth Planet. Sci. Lett. 584, 117500.
Weidendorfer, D., Schmidt, M.W., Mattsson, H.B., 2017. A common origin of carbonatite magmas. Geology 45, 507–510.
Williams, L.A.J., 1982. Physical Aspects of Magmatism in Continental Rifts Volume 8. In: Pálmason, G. (Ed.), Continental and Oceanic Rifts, American Geophysical Union, Washington, pp. 193–222.
Wilson, M., Rosenbaum, J.M., Dunworth, E.A., 1995. Melilitites: partial melts of the thermal boundary layer? Contrib. Mineral. Petrol. 119, 181–196.
Wölbern, I., Rümpker, G., Link, K., Sodoudi, F., 2012. Melt infiltration of the lower lithosphere beneath the Tanzania craton and the Albertine rift inferred from S receiver functions. Geochem. Geophys. Geosyst. 13, Q0AK08.
Yaxley, G.M., Anenburg, M., Tappe, S., Decree, S., Guzmics, T., 2022. Carbonatites: Classification, Sources, Evolution, and Emplacement. Annu. Rev. Earth. Planet. Sci. 50, 261–293.
Yoder Jr., H.S., 1975. Relationship of melilite-bearing rocks to kimberlite: a preliminary report on the system akermanite-CO_2. Phys. Chem. Earth 9, 883–894.
Zou, H., Zindler, A., 1996. Constraints on the degree of dynamic partial melting and source composition using concentration ratios in magmas. Geochim. Cosmochim. Acta 60, 711–717.